



Universitat Autònoma De Barcelona

Faculty of Sciences  
Modeling for Science and Engineering

---

## Mathematical techniques in visualizing data

---

*Author:*  
Samar Moussa

*Supervisor:*  
Dr. Jozsef Farkas

Dissertation submitted for the degree of  
**Master of Science in (*Modeling For Science and Engineering - Data Science  
specialization*)**

**September 2022 - 2023**



# Abstract

---

This master's thesis investigates the efficacy of mathematical transform, and to be specific, Radon transform, in the visualization and reconstruction of medical imaging data.

Extensive research has been conducted on various mathematical techniques, such as the Radon transform, Fourier transform and many other transforms, including their applications, mathematical notations, and implementation using Python for medical images processing. Python provides image processing tools that enable manipulation, comparison, and restoration of multiple datasets of medical images across different modalities.

Mathematical transforms play a crucial role in medical image processing by enhancing diagnostic accuracy, improving image quality, and increasing efficiency. These advancements are vital for driving innovation in the medical field and aiding doctors and researchers in early disease diagnosis and detection.

By employing mathematical techniques, medical scientists can identify areas that require improvement. This thesis introduces and discusses different types of medical imaging and the associated data visualization and a reconstruction technique employed for these modalities. It focuses on the reshaping of medical images using mathematical tools, such as the inverse Radon transform, and compares the results by studying the accuracy rate with three statistical measurements.

While the reconstructed medical images may appear similar to the human eye, this thesis demonstrates that a statistical analysis reveals significant differences. It elucidates the importance of these disparities to researchers and data scientists, as they contribute to improving the accuracy of medical imaging for enhanced diagnosis.

Through a comprehensive exploration of mathematical tools used in visualizing medical imaging data, this thesis aims to contribute to the advancement of diagnostic accuracy and clinical decision-making processes. By leveraging the power of mathematics, medical professionals can gain valuable insights from imaging data, leading to improved patient care and outcomes in the realm of medical imaging.

In this thesis, we investigate the efficacy of employing the Radon transform and its inverse to reconstruct medical images in the DICOM format. The study assesses variations in image quality and accuracy between original and recon-

structed images while emphasizing the significance of mathematical transforms in the medical image reconstruction process, specifically through applying the inverse Radon transform to three types of medical images (CT scans, MRI, and PET). The accuracy rate was examined through the utilisation of statistical approaches, namely structural similarity index measure (SSIM), mean squared error (MSE), and peak signal to noise ratio (PSNR).

Utilizing the inverse Radon transform, medical images of diverse modalities were successfully reconstructed. A comparative analysis between the original and the reconstructed images indicated superior accuracy rates across three distinct metrics when using phantom medical images, primarily due to the absence of noise.

Employing the inverse Radon transform has demonstrated promising results in reconstructing three distinct types of medical images, each varying in usage and structural intricacies. However, it was observed that the computational time required to process merely 44 medical images from each dataset was relatively prolonged, particularly given the simplicity and absence of color in the images. This raises concerns about time efficiency when handling more extensive datasets, especially in substantial medical establishments. Furthermore, there exists potential to enhance performance by integrating convolutional neural networks (CNN) with the inverse Radon transform, leveraging more extensive training datasets, and advanced filtering techniques. Conclusively, the employment of phantom medical images emerges as the optimal dataset selection, as evidenced by the results. Specifically, PET scans, where the phantom image dataset is utilized, exhibit superior image reconstruction quality across all three evaluation metrics. CT reconstructions are commendable, trailing closely behind. Meanwhile, MRI reconstructions, although demonstrating notable signal strength (PSNR), manifest increased errors (MSE) and structural discrepancies (SSIM).

# Acknowledgements

---

With a profound sense of gratitude, I extend my heartfelt gratitude to those who have played a vital role in shaping my academic journey:

At the forefront, I wish to express my deepest thanks to Professor Jozsef Frakas. His consistent guidance, unwavering support, and patient involvement have been pivotal in sculpting the trajectory of my thesis preparation. The invaluable insights he has provided through his constructive feedback have significantly deepened my understanding of this topic.

I am deeply honored to convey my sincere gratitude to:

Professor Anna Cima Mollet, her constant support throughout our master's program and her unceasing encouragement since my study in Spain commenced have illuminated my path and been a wellspring of motivation, propelling me forward.

Further, I extend my heartfelt appreciation to Professor Judit Chamorro for her valuable insights during the Optimization course. Her meticulous guidance has been pivotal in shaping my academic growth.

A heartfelt thank you is due to Professor Àngel Calsina for generously sharing his time and expertise as a committee member during my thesis presentation.

A debt of gratitude is owed to my fellow classmates and office companions, whose steadfast support has served as a pillar of strength during the most challenging of times. The unflinching encouragement from my cherished friends has provided unwavering solace and motivation.

The appreciation I hold for all the professors who have contributed to my educational journey is immeasurable. Their dedication to imparting knowledge has enriched my academic experience in countless ways.

I wish to express my deep thanks to FAS and Jusoor organization, especially Mrs. Sarah Shedeed and Ms. Marta Batalla Calavia. Their belief in my potential, as manifested through Jusoor-UAB scholarship, has provided the wings that carried me to this significant milestone.

Concluding, I reserve a special gratitude for my family. Their unyielding belief in my potential has been the cornerstone of my journey. Their constant encouragement and the values they have instilled have collectively shaped me into the individual I am today. Their presence remains a perennial source of inspiration, and they eternally inhabit my thoughts and memories.

# Contents

---

<b>Abstract</b>	<b>i</b>
<b>Acknowledgements</b>	<b>iii</b>
<b>1 Introduction</b>	<b>2</b>
1.1 Challenges facing medical imaging and data visualization in general . . . . .	2
1.2 Objectives of the study . . . . .	4
1.3 Methodology . . . . .	4
1.4 Achievements . . . . .	5
<b>2 Background</b>	<b>6</b>
2.1 The history of medical imaging modalities . . . . .	6
2.2 Medical imaging processes . . . . .	8
<b>3 Therotical concepts</b>	<b>10</b>
3.1 Mathematical transforms . . . . .	10
3.2 Important mathematical transforms in medical imaging - Radon transform . . . . .	10
3.2.1 Reconstructing medical images using Radon transform .	13
3.3 Important mathematical transforms in medical imaging - Fourier transform . . . . .	15
3.3.1 Reconstructing medical images using Fourier transform .	16
3.4 Other mathematical methodologies - statistical techniques . . . . .	16
3.4.1 Principal component analysis (PCA) . . . . .	16
3.4.2 Singular value decomposition (SVD) . . . . .	18
<b>4 Medical imaging</b>	<b>20</b>
4.1 Medical images and their processing techniques . . . . .	20
4.1.1 X-ray . . . . .	21

4.1.2	Magnetic resonance imaging (MRI) . . . . .	22
4.1.3	Computed tomography (CT) . . . . .	24
4.1.4	Ultrasound images . . . . .	25
4.1.5	Positron emission tomography (PET) . . . . .	27
4.1.6	Single-photon emission computed tomography (SPECT) .	30
<b>5</b>	<b>Technical chapters</b>	<b>32</b>
5.1	Reconstructing medical imaging using transforms . . . . .	32
5.2	Methodology . . . . .	32
5.2.1	Used algorithm . . . . .	33
5.2.2	Python implementation . . . . .	34
<b>6</b>	<b>Results and discussions</b>	<b>38</b>
6.1	Dataset used and description . . . . .	38
6.1.1	CT dataset . . . . .	38
6.1.2	MRI breast cancer dataset . . . . .	38
6.1.3	PET phantom dataset . . . . .	39
6.2	Results . . . . .	39
6.2.1	Interpretation of the mean squared error (MSE) results .	39
6.2.2	Interpretation of accuracy . . . . .	40
6.3	Results interpretation . . . . .	40
6.3.1	CT scan . . . . .	40
6.3.2	MRI scan . . . . .	41
6.3.3	PET scan . . . . .	41
6.4	Discussions . . . . .	41
<b>7</b>	<b>Conclusions &amp; future work</b>	<b>42</b>
7.1	Conclusions and results . . . . .	42
7.2	Challenges within this work . . . . .	43
<b>Appendix 1 - Implementation code</b>		<b>49</b>

<b>Appendix 2 - Plotting results with MSE</b>	<b>51</b>
<b>Appendix 3 - Statistical accuracy metrics used</b>	<b>55</b>
<b>Appendix 4 - Plotting accuracy results</b>	<b>57</b>

# List of Figures

---

2.1	Modalities of medical images [1] . . . . .	7
2.2	Medical image processing techniques [2] . . . . .	9
4.1	X-ray of a COPD case [3] . . . . .	22
4.2	MRI of a normal brain [4] . . . . .	24
4.3	CT scan during Covid19 [5] . . . . .	26
4.4	Ultrasound of the liver [6] . . . . .	27
4.5	PET scans image example [7] . . . . .	29
4.6	SPECT 3D for liver [8] . . . . .	31
5.1	Accuracy metrics comparison. . . . .	37
7.1	MSE average for each dataset . . . . .	50
7.2	Original and reconstructed images results for CT . . . . .	53
7.3	Original and reconstructed images results for MRI - example 1 .	53
7.4	Original and reconstructed images results for MRI - example 2 .	54
7.5	Original and reconstructed images results for phantom PET scan	54
7.6	MSE, PSNR and SSIM accuracy . . . . .	56
7.7	Accuracy measurement among datasets . . . . .	58

# 1

## Introduction

---

### 1.1 Challenges facing medical imaging and data visualization in general

Medical and CT scan data are considered one the most complex and difficult type of data that is hard to interpret since it is primarily consists of a visual representation to the body, brain or bone tissue using black and white spectrum color. Having complex interpretation of these medical images makes it challenging for medical professionals to accurately diagnose and treat patients.

Therefore, the urgent need for effective mathematical techniques for visualizing medical and CT scan data is crucial and necessary.

In general, medical imaging is used in medicine for multiple purposes including diagnosis, treatment plans, and to monitor disease progression. However, interpreting medical images can be difficult as such type of images involve complex structures and require knowledge of both anatomy and pathology especially in CT scans.

CT scans produce detailed images of internal structures which, without the proper training, is hard to read and explain. These images are usually in (DICOM) format, which is basically a medical imaging format stands for "The Digital Imaging and Communication In Medicine" used specifically for biomedical images and image-related information since this type of images is better for an effective network communication and connectivity between different departments in medical centers and hospitals. [9]

One of the main challenges in modern medical imaging nowadays is the need for accurate and reliable image analysis. This step is crucial in order to make meaningful diagnoses and treatment decisions. This procedure facilitates the

identification and quantification of several characteristics included in the images, including the dimensions and spatial coordinates of tumours or the extent of damage to tissue in case of incidents. This requires a thorough understanding of the anatomy and pathology along with the ability to use advanced mathematical techniques to analyze the images which might be faster and more detailed.

Another challenge to mention in medical imaging is the need for standardization and interoperability. First of all, medical images are often produced by different devices and in multiple formats, making it harder to compare images from different sources or to integrate them into a single patient record. The DICOM standard was developed to address this issue as well, providing a common format for medical images and a unified standard set of metadata for describing such images.

Despite these challenges, advances in medical imaging technology have led to significant enhancements in the identification and management of numerous disorders. For example, currently, CT scans have become a standard practise for the purpose of lung cancer screening and the continuous monitoring of disease advancement in individuals diagnosed with chronic obstructive pulmonary disease (COPD). In addition, the utilisation of MRI has emerged as a fundamental technique in the realm of monitoring and diagnosing brain and other serious injuries, and it is still used for identifying abnormalities in the heart and other organs.

To further improve the reliability of medical imaging, researchers are developing new mathematical techniques for image analysis and interpretation. These techniques include machine learning algorithms, which can be used to detect and cluster, and classify the type and number of features used in medical images, along with the prediction of the possibility of a tumor progression based on the medical data of a patient. Furthermore, advanced mathematical models like transforms, which we will explain later on in this thesis can also be used to simulate the behavior of tissues and organs in response to another different stimuli.

To further explain transforms, programming languages have interfered to facilitate the process of using mathematical models and machine learning. For this reason, in the thesis we will use Python as the programming language to apply to the study for effectiveness of inverse Radon transform in multiple medical datasets.

Python has emerged as a powerful tool for implementing these techniques, with a number of libraries available for image processing, data interpretation and analysis, machine learning, and scientific computing. By combining these tools with a deep understanding of the underlying mathematics behind the medical images, researchers can continue to make significant improvements

in the clinical field, improving our ability to diagnose and treat disease and ultimately patient's health and well-being.

## 1.2 Objectives of the study

The objective of this thesis is to explore various mathematical techniques for visualizing and reconstructing medical images including Fourier transform, Radon transform and its inverse. In addition, studying the effectiveness and accuracy of using the inverse Radon transform in the reconstruction of three different medical images datasets which include CT scans, MRI's and PET.

## 1.3 Methodology

The goal of this thesis is to study the effectiveness of the inverse Radon transform in reconstructing medical images from different types and checking the accuracy level of using this transform. In order to achieve this purpose, First step is to collect the medical images from different types and gather them in different datasets, knowingly that DICOM image type are the common original standard for medical images, hence, all of the medical images used in this thesis will be provided using this format for the purpose of facilitating reading and visualizing these images. Furthermore, since the original images used in this thesis are derived from the Cancer Imaging Archive , the original format is TCIA format, and in order to have all the images used unified in one format which is the DICOM standard, we will use a software tool provided by the cancer imaging archive website called NBIA Data retriever to help reformulate all of the images into .dcm or DICOM format . [10]

After that, using python pydicom library, multiple functions will be applied to read, analyze, visualize and process these images.

The next step is followed by extracting the sinogram pixel by pixel values for each type of images (CT, MRI, PET) for building a reconstructed version of the image we are dealing with. Third step is introducing the mathematical techniques such as linear and integral transforms to visualize the data and here the inverse Radon transform will be applied. The techniques are compared and evaluated based on their effectiveness in identifying anatomical structures and abnormalities in the medical data from different image types a purposes. In this thesis, the evaluation of the effectiveness is conducted by calculating the accuracy using the MSE (mean squared error) to check the level of effectiveness for each image reconstructed compared to the original image along. Moreover, because to the potential insufficiency of relying just on this

measurement, we will incorporate additional statistical metrics such as the structural similarity index (SSIM) to ascertain whether the visual perception aligns with the outcomes of this transform and the peak signal to noise ratio (PSNR) to prove whether what appears to the human eye is the same result of this transform or not.

## 1.4 Achievements

The research identifies several mathematical techniques that are considered effective in visualizing medical and CT scan data.

The inverse Radon transform is found to be useful for visualizing the internal and external structures of organs for a single image in almost significantly no time with a MSE less than 20 percent, which is good considering that this inverse transform is hard to achieve perfectly with zero errors.

But, when this transform is applied to multiple datasets of several images, it has a high computational complexity execution and this requires more time to acquire the results which can affect the efficiency of a medical facility in case applied in real-life. Furthermore, the usage of phantom medical images eliminates the noise to the minimal amount possible which is shown in our study.

The registration and segmentation of the medical images are considered significantly important mathematical steps to analyze medical images in detail, isolate and study specific body regions of interest. However, statistical analysis and transforms are crucial in medical image visualization and reconstruction as they facilitate the identification of patterns, correlations within the data, and areas of improvement, so their utility becomes apparent.

Overall, the research achieves the objective of exploring and developing effective mathematical techniques for visualizing different medical and CT scan data using the inverse Radon transform, which can potentially lead to better diagnoses and treatments for patients and spots the light on the most important measurements of accuracy, images quality and extensions to be used while studying the effectiveness of mathematics in medicine.

# 2

## Background

---

### 2.1 The history of medical imaging modalities

Medical imaging has become deeply integrated into modern medicine over the past three decades, serving as a significant milestone and transforming the delivery of healthcare and the medical field. [11]

This advancement has greatly benefited individuals and professionals worldwide. The field of radiography and the subsequent development of the medical imaging industry may be traced back to the seminal discovery of X-rays by Nobel laureate Wilhelm Roentgen. [11]

The utilisation of medical imaging is facilitating a more advanced era of diagnosis by enhancing human visual perception to gain deeper insights into the fundamental nature of diseases. In pursuit of this objective, the obtained images not only function as an indicator of the level of worsening in a patient's illness and the extent of their recovery process, but also significantly help to facilitating accurate clinical decision-making. There is currently a growing demand for effective management systems to assure the preservation, safety, and retrieval of data in the future. [11]

In 1895, the inception of medical imaging had been attributed to the fortuitous discovery of X-radiation by Röntgen. X-radiation, which consists of X-rays as a type of electromagnetic radiation, possesses the capability to discern and delineate bone structures. As a result, X-rays have been largely utilised in the realm of healthcare and medical imaging, specifically in the domains of oral healthcare and thoracic examination. [11]

After years of working with X-rays, and in response to the inherent constraint and limitations of X-rays providing solely two-dimensional perspectives, the development of X-ray computerised tomography (CT) emerged throughout the 1970s. This innovative technique harnessed computer processors to build

comprehensive three-dimensional representations of an object's internal structure.

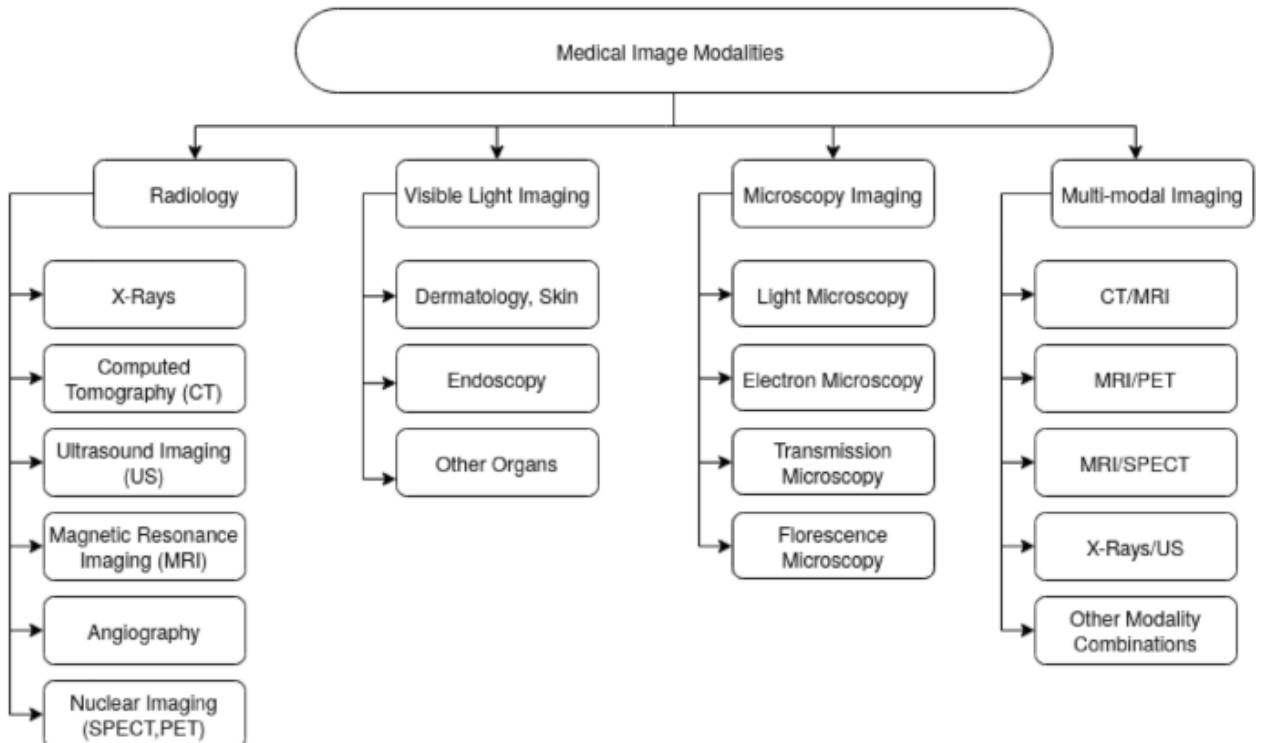


Figure 2.1: Modalities of medical images [1]

While computed tomography (CT) has been commonly utilised in the examination of the human brain, its limitations in investigating brain processes have led to the emergence of positron emission tomography (PET) and single photon emission computed tomography (SPECT) as alternative imaging techniques.

Positron emission tomography (PET) is a nuclear medicine imaging technology that enables the collection of three-dimensional visualisations or functioning illustrations of biological processes. This form of imaging delivers insights into the structure and operation of tissues and organs within the body. [11]

Generally, medical images are inherently diverse, encompassing several domains such as cardiac medical images, brain, and others. In each domain, many imaging modalities can be utilised to obtain images, as discussed in the aforementioned context. Furthermore, the management of medical imaging data encounters significant challenges due to the vast volume of images generated on a daily basis, making effective management infeasible in several respects.

## 2.2 Medical imaging processes

After discussing the progression of medical imaging modalities, it is crucial to consider the various stages involved in processing medical images. These stages encompass registration, segmentation, and reconstruction. The latter serves as a mean for visualising medical images. A thorough understanding of the mathematical transforms employed in the progression of medical images is required for effective results in image processing. [1]

The diagram presented in Figure(2.2) below elucidates the methodology by which medical image processing techniques can be utilised and implemented.

The process begins with the acquisition of images from many sources. Subsequently, preprocessing is conducted, involving the removal of noise and the application of filtering techniques and enhancement the filters to diminish undesired features and further reduce noise. Segmentation is a crucial step in medical therapy and evaluation, as it involves assigning labels to known pixels. This process results in the formation of segmented objects, where pixels with the same label are grouped together.

The following point of discussion is registration which is a process that involves coordinating the spatial location of one or more images in order to establish a shared coordinate system. Label transfer is a widely employed technique in population analysis for the purpose of picture segmentation, as it is deemed to be of utmost importance. The objective is to identify anatomical or functional sites that correspond to each other in two or more photographs. Image registration can be utilised for aligning images acquired from a range of imaging modalities at different time intervals within the same subject, as well as for aligning images taken from distinct subjects. In order to achieve picture registration, it is typically required to estimate a geometric transformation that aligns the images. [12]

In this thesis, we will be focusing more on the medical image processing visualization and taking into consideration each imaging modality by itself in terms of reconstructing medical images. [13]

The reconstruction of images is a fundamental component within several systems of visual perception. This involves the process of dividing multiple segments or objects using visual representations with the primary objective being to get high-quality medical images for clinical purposes while minimising costs and risks to patients. [13]

Image reconstruction is a computational approach that involves the integration of two-dimensional images into a computer system. Afterwards, the image is subjected to a series of transforms aimed at boosting and assessing its

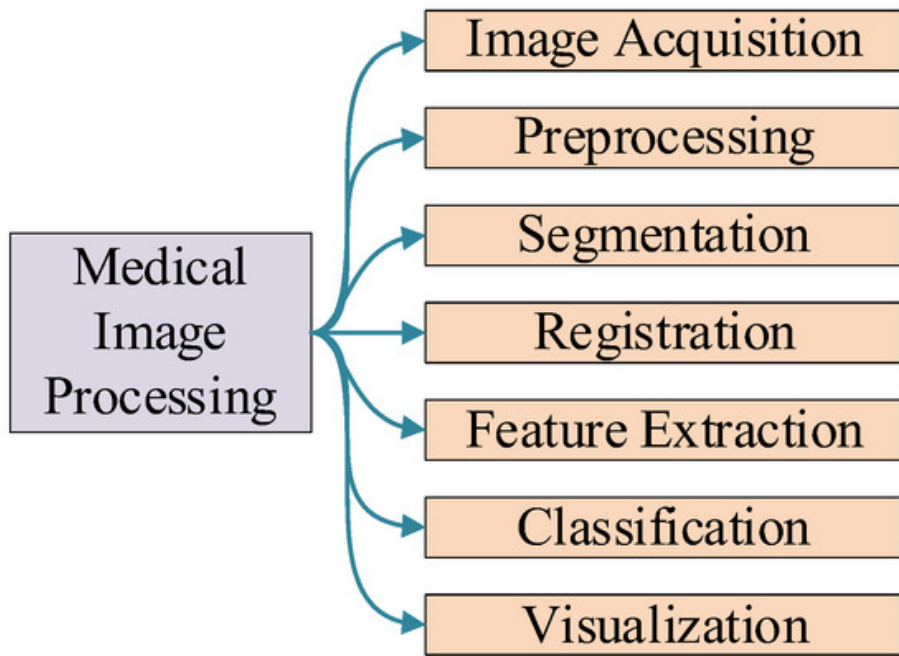


Figure 2.2: Medical image processing techniques [2]

quality and facilitating the examination of medical procedures performed on patients. [13]

Therefore, it is imperative to ascertain the reconstruction approaches, which pertain to the methodologies utilised in order to recover the original optimal image from a provided image. To explain further, two-dimensional photos are read digitally through a computer and afterwards enhanced or explored to transform the image to enhance the practicality and use for human observers, the provided image can be reformulated in an applicable manner. [13]

In the realm of image reconstruction, two predominant approaches exist: analytical and iterative reconstruction. In this thesis, we will have a thorough example on the effectiveness of the analytical reconstruction using the Radon and inverse Radon transform. [13]

Although convolutional neural networks (CNNs) are often considered the optimal choice for image reconstruction, multiple research papers indicate that the currently employed CNN techniques require additional data training to achieve results comparable to those obtained by current analytical reconstruction techniques with appropriate sampling. [13]

# 3

## Theretical concepts

---

### 3.1 Mathematical transforms

To begin with, it is important to understand the purpose and definition of a transform. Mathematical transforms are used to extract additional information from signals that are not immediately discernible in their original form. There are various transforms that can be employed, with the Fourier transform being widely recognized as the most prevalent one.

Within the topic of this thesis, the Radon transform is well recognized as the predominant mathematical technique employed in the field of medical imaging reconstruction. The Radon transform is a mathematical integral transform that establishes a mapping between a function  $f$  defined on a two-dimensional plane to a function  $Rf$  defined on a set of lines in the plane. The numerical representation of  $Rf$  at a specific line is equivalent to the line integral of the  $f$  along that line. The Radon transform was first introduced in 1917 by Johann Radon, who also derived a formula for its inverse transform. [14] [15] [16]

### 3.2 Important mathematical transforms in medical imaging - Radon transform

In the world of medical imaging, and to be exact, in our thesis discussion on the usage of mathematics in constructing medical images, the list of mathematical transforms is a little bit limited. The transforms that have been used in this field are mostly linear transforms, which include: Radon transform, Fourier transform, and Abel transform.

There are multiple applications for transforms in medical imaging. These applications are divided into segmentation, classification, detection, recon-

struction, synthesis, registration, report generation, and other applications as well. [17]

There are numerous mathematical ways for representing medical imaging, with particular significance placed on certain transforms within the health-care domain. In this discussion, we will focus on two prominent transforms: the Radon Transform and the Fourier Transform. To explain more about each transform and their usage, we will start with the Radon Transform, which is considered generally as a mathematical technique employed to represent the data acquired via tomographic scans. The original projection qualities can be reconstructed by employing the inverse of the Radon transform. This capability proves valuable in various fields such as computed axial tomography or (CAT), and solving hyperbolic partial differential equations. [16]

Radon Transform can be defined as the following:

Consider a function  $f(\mathbf{x}) = f(x, y)$  that fulfils the three regularity conditions [15]:

These assumptions or conditions are set for the mathematical function to operate effectively to ensure that the transform is well-defined and can be reliably inverted to reconstruct the original function. They pertain to the smoothness and decay of the function being transformed. These assumptions are critical and crucial in practice. For example, in CT scan cases, we want to ensure that the inverse Radon transform provides a meaningful and accurate representation of the original function or object and the regularity conditions provide such accuracy. [18]

These regularity conditions in case of Radon transform case are:

1.  $f(\mathbf{x})$  a mathematical function that exhibits the property of continuity.
2. The expression for the double integral is provided as:

$$\iint \frac{|f(\mathbf{x})|}{\sqrt{x^2 + y^2}} dx dy$$

3. For any random point  $(x, y)$  on the plane, it is considered true that [15]:

$$\lim_{r \rightarrow \infty} \int_0^{2\pi} f(x + r \cos \varphi, y + r \sin \varphi) d\varphi = 0.$$

With the satisfaction of these three conditions, the Radon transform,  $Rf$ , is a function defined on the space of straight lines  $L \subset \mathbb{R}^2$  by the line integral along each such line as [16] [15]:

$$Rf(L) = \int_L f(\mathbf{x}) |d\mathbf{x}|.$$

The equation representing a straight line  $L$  in terms of arc length  $z$  can be expressed as [16]:

$$(x(z), y(z)) = (z \sin \alpha + s \cos \alpha, -z \cos \alpha + s \sin \alpha),$$

The variable  $s$  represents the distance of  $L$  from the origin, whereas  $\alpha$  represents the angle that the normal vector to  $L$  forms with the X-axis. It follows that the quantities  $(\alpha, s)$  can be considered coordinates on the space of all lines in  $\mathbb{R}^2$ , and the Radon transform can be expressed in these coordinates by [16]:

$$Rf(\alpha, s) = \int_{-\infty}^{\infty} f(x(z), y(z)) dz = \int_{-\infty}^{\infty} f(z \sin \alpha + s \cos \alpha, -z \cos \alpha + s \sin \alpha) dz.$$

In the context of a  $n$  dimensional space  $\mathbb{R}^n$ , it is generally observed that, the Radon transform of a function  $f$  which fulfils the aforementioned regularity requirements, is a function  $Rf$  on the space  $\Sigma_n$  among all hyperplanes in  $\mathbb{R}^n$ . The term is characterised by [16]:  $Rf(\xi) = \int_{\xi} f(\mathbf{x}) d\sigma(\mathbf{x}), \quad \forall \xi \in \Sigma_n$

The importance of the Radon transform came from the need to use mathematics in the reconstructed tomography. This transform is used to facilitate the process of visualizing and reconstructing medical imaging. Furthermore, it is the process of changing from  $n$  dimensional levels to  $(n-1)$  dimensional line integrals.

For the part of reconstructing medical images, we will have to use the inverse Radon transform which is basically the reverse process of the Radon transform, to obtain the original image in the  $n$  dimension from  $(n-1)$  line integrals. The inverse Radon transform is given using this formula:

$$f(\mathbf{x}) = \int_0^{\pi} (\mathcal{R}f(\cdot, \theta) * h)(\langle \mathbf{x}, \mathbf{n}_\theta \rangle) d\theta \quad (3.1)$$

where  $h$  has a Fourier transform given by  $\hat{h}(k) = |k|$ . The convolution kernel  $h$  which is a fundamental component in image processing and computer vision algorithms and often called the Ramp filter. [16]

The Radon transform quantifies the aggregate of function values along straight trajectories. After capturing these projections during a CT scan, the data are often interspersed with high-frequency perturbations. Additionally, to refine the final image and counteract these irregularities, filters are employed in the frequency domain. The Ramp filter stands out as an important example. [19]

Mathematically, the frequency representation of the Ramp filter is:

$$H(f) = |f| \quad (3.2)$$

where  $f$  is the frequency.

In essence, the inverse Radon transform, employed for the purpose of picture reconstruction from its projections, may result in a fuzzy appearance of the raw back-projected image. The blurring phenomenon can be attributed to the intrinsic characteristics of the Radon transform. In order to mitigate the effects of image blurring and enhance the clarity of the reconstructed image, a frequency domain filter is employed prior to the process of back-projection. The term "Ramp filter" is frequently used to describe this particular filter. Ramp is used as the name of this filter due to its frequency response's resemblance to a rising incline, it initiates from zero and proceeds with a linear gradient corresponding to frequency. [20] [19]

### 3.2.1 Reconstructing medical images using Radon transform

In medical imaging, the Radon transform is used in various imaging modalities such as X-ray, CT scans and SPECT scans. The technique is used to reconstruct an image of the internal structure of the patient from the attenuation of X-rays or gamma rays that pass through the body at different angles.

The Radon transform is formally defined as the integral along a line of a given function  $f(x, y)$  along a line that passes through the point  $(x, y)$  in the plane, with integration performed over all possible lines passing through the plane, where  $R_\theta(s)$  is the Radon Transform of the function  $f(x, y)$  along a line that makes an angle of  $\theta$  with the X-axis and passes through a distance  $s$  from the origin, and  $\delta$  is the Dirac delta function.

The application of the Radon transform in medical imaging allows for the acquisition of a visual depiction of the interior anatomical composition of the patient from projections taken at different angles. The projections are obtained by rotating the X-ray or gamma ray source around the patient and measuring the attenuation of the rays at each angle. The utilisation of the inverse Radon transform afterwards enables the reconstruction of an image depicting the interior structure of the patient based on the acquired projections.

The following steps could create the full picture of the process of reconstruction using Radon transform.

Firstly, process begins with obtaining projections:

Knowing this, we will have to identify what a projection is the negative logarithm of the fractional X-ray transmittance of the object.

The projection function represents the difference between the same angles of the defined space and the the same space with the object in it. The source is placed around the Y-axis and the detector is placed along the X-axis, we will have to perform a parallel projection along the detector system.

However,one of the downsides of medical imaging is that some medical images can provide the projection only by using a density function of the form  $f(x, y)$ .

In general, in order to perform the reconstruct of the medical images, first, projections must be collected at every angle ( $\theta$ ).

With the displacement  $r$  provided assuming we have an object placed in a 2D space  $(x, y)$  and this projection that is collected for every angle along the detector is called the Radon Transform:  $P_\theta(r)$

However, the object can have many values of coordination coefficients and this will create a certain profile based on the attunated photons.

The objective of this function is to reverse the process, to be able to reconstruct the original image.

After a thorough explanation regarding projection, the process begins with the body exposed to a series of X-ray beams that traverse it from various angles. The attenuation of these beams is influenced by the density and content of the tissues they traverse, leading to the formation of projections. [20]

Then, the process is followed by the utilisation of the Radon transform that computes the integral of a function, often known as an image, along straight lines. This methodology facilitates the generation of image projections from a comprehensive range of angles which are called sinograms.

Lastly, the reconstruction of the original images by the utilisation of the inverse Radon transform.

The original image is obtained by transforming the acquired projections (sinograms) back using techniques such as filtered back projection (FBP) which its process consists of two primary stages: filtration along with back projection.

During the filtering phase, the projection data undergo a shift or a transform into the frequency domain, through the utilisation of the Fourier transform most of the time. The data that has been modified is subsequently subjected to multiplication by a filter, typically known as the ramp filter, in order to compensate for the blurring effect caused by the fundamental back projection

method. Subsequently, the filtered data is subjected to another transformation process that restores it to its original spatial domain, yielding a set of projections that have undergone the filtering procedure. During the back projection step, the filtered projections go under a process of smearing, also known as "back projection", across the image plane in order to recreate the initial image. Lastly, the spatial picture is obtained by applying the inverse Radon transform. [20]

In summary, the Radon transform is a highly influential mathematical tool employed in the field of clinical imaging for the purpose of acquiring a visual depiction of the interior composition of a patient from projections taken at different angles. The technique has numerous applications in various imaging modalities and plays a super important role in the diagnosis.

### **3.3 Important mathematical transforms in medical imaging - Fourier transform**

In medical image analysis, the Fourier transform serves as a cornerstone for transitioning from the spatial to the frequency domain. This transition bestows the capability to dissect and manipulate the spectral components of an image, revealing nuanced characteristics often imperceptible in the spatial representation.

The Fourier transform serves as a critical mathematical tool utilized to transition signals or images between their time (or spatial) and frequency domains, finding vast applications in fields such as physics and engineering. In other words, if  $f$  represents the function being transformed, the resulting function  $F$  after performing the transform is termed the Fourier spectrum.

While the Fourier transform typically transforms complex-valued functions into other complex-valued functions, in image transform, the challenge is to represent a complex function  $F$  as a real function. A typical method involves computing the real function as the squared magnitude of the complex function  $F$  and subsequently portraying it graphically.

For understanding image structures, the Fourier transform proves invaluable importance extensively in scientific literature. This is a one-dimensional demonstration of the Fourier transform's operation, given by:

$$F(\nu) = \int_{-\infty}^{\infty} f(x) \exp(-i2\pi x\nu) dx \quad (3.3)$$

Where  $f(x)$  represents the function under study,  $\nu$  denotes the spatial frequency, and  $i$  is the imaginary unit.

In other words, Fourier transform can be used to analyze the frequency content of an image. It decomposes the image into its component frequencies and allows for the separation of low frequency and high-frequency information.

### **3.3.1 Reconstructing medical images using Fourier transform**

Since the thesis focus is on using the inverse Radon transform to perform the reconstruction of medical images, we will briefly mention here the steps used in order to reconstruct these images using Fourier transform for the purpose of possibility of performing further reconstruction in higher dimensions. [21]

Firstly, the direct measurement of spatial images is not performed by MRI, instead, it gathers data in the frequency domain, frequently denoted as k-space.

The k-space data undergoes a two-dimensional Fourier transform. The aforementioned procedure facilitates the conversion of data from the frequency domain to the spatial domain, resulting in the generation of an image that can be readily interpreted.

Lastly, the process of post-processing refers to the manipulation and enhancement of digital images. Frequently, additional processing is used to the rebuilt image in order to augment fine details or mitigate artefacts. This can encompass operations conducted in both the spatial and frequency domains. [21]

## **3.4 Other mathematical methodologies - statistical techniques**

### **3.4.1 Principal component analysis (PCA)**

PCA is a statistical technology primarily used for data analysis along with dimensionality reduction. It identifies the most important features of a dataset and transforms it into a new coordinate system, where the data can be visualized and analyzed more efficiently. [22]

PCA is based on the concept of eigenvectors and eigenvalues. It finds a set of orthogonal vectors, called principal components, that represent the underlying structure of the data. The initial principle component signifies the direction in which the data exhibits the greatest amount of variation, whereas each

consecutive principal component symbolises the direction in which the data exhibits the greatest amount of variation that is perpendicular to the previous components. The eigenvalues associated with each principal component represent the amount of variation explained by that component.

PCA is widely used in medical imaging to reduce the dimensionality of large datasets and extract meaningful information. It is a versatile technique that can be employed in several applications within the field of medical imaging, including feature extraction, segmentation, and visualisation, similar to MRI, PET scan, and CT scans which we are going to use in our technical chapter for the reconstruction process of the medical images.

One of the main advantages of PCA is that it enables the identification of the most important features of a dataset. This can be especially useful in medical imaging, where large datasets can contain a lot of noise and irrelevant information. PCA can also help reduce the computational burden of processing large datasets by reducing the dimensionality of the data.

However, PCA also has some limitations. One of the main challenges is the interpretation of the results. The principal components may not always correspond to meaningful features of the data, and it can be difficult to interpret the results in a clinically relevant manner. Additionally, PCA assumes that the data is normally distributed, and may not be suitable for non-Gaussian data.

Mathematically, the PCA transformation can be represented as follows:

Let  $X$  be a matrix of  $n$  observations and  $m$  variables, where each row represents an observation and each column represents a variable. The PCA transformation can be performed by first centering the data by subtracting the mean of each variable from each observation. Then, the covariance matrix  $C$  of the centered data is computed. The eigenvectors and eigenvalues of  $C$  are then calculated, and the data is transformed into the new coordinate system defined by the eigenvectors.

$$C = \frac{1}{n-1}(X - \bar{X})^T(X - \bar{X}) \quad (3.4)$$

$$\lambda_i \mathbf{v}_i = C \mathbf{v}_i \quad (3.5)$$

$$Y = X\mathbf{V} \quad (3.6)$$

where  $\lambda_i$  and  $\mathbf{v}_i$  are the eigenvalues and eigenvectors of  $C$ , respectively,  $\bar{X}$  is the mean of  $X$ , and  $Y$  is the transformed data matrix. [23]

Given matrix  $X$  which is  $n \times m$  (with  $n$  observations and  $m$  variables), the mean

$\bar{X}$  of  $X$  is a row vector of size  $1 \times m$ . Each element of  $\bar{X}$  is the mean of the corresponding column of  $X$ .

Mathematically, the mean  $\bar{x}_j$  of the  $j$ -th column of  $X$  is calculated as:

$$\bar{x}_j = \frac{1}{n} \sum_{i=1}^n x_{ij}$$

Where:

- $\bar{x}_j$  is the mean of the  $j$ -th column.
- $x_{ij}$  is the element in the  $i$ -th row and  $j$ -th column of  $X$ .

Putting it all together, the mean matrix  $\bar{X}$  is:

$$\bar{X} = [\bar{x}_1, \bar{x}_2, \bar{x}_3, \dots, \bar{x}_m]$$

In summary, PCA is a powerful statistical technique used for dimensionality reduction and data analysis. It can be used to identify the most important features of a dataset and transform it into a new coordinate system for visualization and analysis. PCA has numerous applications in medical imaging, but also has some limitations that must be considered when applying it in practice. This statistical technique is used to reduce the dimensionality of an image by identifying the most important features. It can be used for image compression and to identify patterns in medical images. [23]

### 3.4.2 Singular value decomposition (SVD)

SVD is a fundamental approach in linear algebra that sheds light on the field of data dimensionality and reduction. SVD has had a substantial influence on the field of medical imaging, namely in the area of reconstruction. [24]

The origins of SVD can be traced back to mathematical efforts to simplify intricate information, despite its divergence from present-day applications.

SVD is articulated mathematically by the relation [25]:

$$A = U\Sigma V^* \tag{3.7}$$

where  $A$  signifies the matrix in question, both  $U$  and  $V^*$  are orthogonal matrices, and  $\Sigma$  is a diagonal matrix encompassing the singular values. Grasping this notation is imperative, serving as the foundation for unraveling its application in the realm of medical image reconstruction. [26] [27] [25] [28]

For a non-squared matrix, the SVD is calculated as follows:

Given a matrix  $A$  of dimensions  $m \times n$ , its SVD is given by:

$$A = U\Sigma V^*$$

Where:

- $U$  is an  $m \times m$  unitary matrix.
- $\Sigma$  is an  $m \times n$  diagonal matrix containing the singular values of  $A$  in descending order on its diagonal.
- $V^*$  is the conjugate transpose of an  $n \times n$  unitary matrix  $V$  (or simply  $V^T$  if  $A$  is a real matrix). [28]

The fundamental utility of SVD resides in its capacity to breakdown a given image into its fundamental characteristics, enabling the reconstruction of images with less noise and enhanced clarity. This is particularly crucial in situations where the initial medical data is lacking.

Leveraging SVD for reconstruction offers several intrinsic benefits which can be summarized in the following points:

- (a) - Diminishing noise is pivotal in medical imaging, emphasizing the need for utmost precision and clarity.
- (b) - Data compression refines complex datasets, rendering them more digestible and straightforward.
- (c) - The refinement in the reconstruction approach bolsters image quality, yielding sharper, more lucid visuals.

To sum up, the landscape of medical imaging has undergone profound transformations with the application of advanced mathematical and statistical techniques. Among these, PCA and SVD stand out for their pivotal roles. [29]

PCA, has enabled extraction of primary components from extensive datasets in medical imaging. This results in more focused and efficient imaging processes while preserving most of the essential variance in data. [29]

Similarly, SVD has become an invaluable tool, especially when addressing problems associated with noise, data compression, and enhancement of image clarity. Its capacity to decompose images into essential features facilitates superior reconstruction, making it indispensable in situations where original data might be fragmented or degraded. [27]

In essence, these mathematical and statistical tools have significantly elevated the standards and outcomes of medical image reconstruction. Their introduction and implementation have not only improved image quality but also amplified the diagnostic precision of these images, thereby enhancing patient care. [27]

# 4

## Medical imaging

---

In chapter 4 of this thesis, we embark on an exploration of the diverse medical imaging modalities prevalent in healthcare establishments. Given the thesis's emphasis on the mathematical intricacies underlying data visualization, our initial focus will be on delineating the varieties of medical images, elucidating their respective utilities, advantages, and their distinct roles in therapeutic contexts. The ensuing chapter promises a deeper dive, elucidating the practical application of mathematical techniques in Python, particularly harnessing the Radon and its inverse transform, tailored to each imaging modality.

### 4.1 Medical images and their processing techniques

Since the evolution of the field of medical imaging, several types of medical images have come to light nowadays because of different treatment purposes, for example, the type of images a patient will receive while scanning their internal organs is different than the type of images used in different parts of the body like the brain or the broken bone tissue and for other specific medical purposes. This difference, has participated in the advancement and was super beneficial for the medical and health sector massively.

Imaging encompasses many diagnostic procedures employed to generate visual illustrations of the body. These images serve the purpose of screening potential health disorders in advance of symptom manifestation, determining the root cause of diseases, and monitoring the progression of health conditions post to diagnosis. Imaging is also known as radiology. There are numerous medical images, with each imaging modality employing distinct technological procedures. These techniques can be used to extract information from medical images to aid in diagnosis and treatment. There are variations in the extent to which they effectively depict the physiological processes occurring within specific bodily tissues depending on the type of injury to identify the best medical image to be used by doctors. [30]

#### **4.1.1 X-ray**

X-ray imaging is a pivotal diagnostic modality that harnesses electromagnetic radiation in order to provide intricate graphical representations of the internal components of the body of an individual. This technique leverages the distinct absorption properties of different body tissues when exposed to X-rays. [31]

During an X-ray procedure, the patient is strategically positioned between the radiography equipment and a sensor. A controlled stream of X-rays is projected through the body. As these rays traverse through, they undergo differential absorption by varying tissues. The residual rays reaching the sensor are recorded and subsequently processed via computational methods to render an insightful depiction of the internal structures.

Historically, the significance of X-ray imaging was pioneered by its discovery in 1895 by Wilhelm Conrad Roentgen. It swiftly metamorphosed into an indispensable medical imaging technique. This modality meticulously discerns the gradients in tissue densities, denser tissues such as bones are rendered in lighter shades, while less dense structures manifest darker. This contrast proficiency makes X-ray imaging the gold standard for detecting bone anomalies, pulmonary conditions, dental irregularities, and even some digestive system abnormalities. Moreover, X-ray imaging can be synergized with advanced computational methods like the Radon transform to refine the acquired images. [31]

A standout virtue of X-ray diagnostics is its widespread availability combined with cost-effectiveness. It offers rapid, non-intrusive diagnostics, typically not necessitating hospital admission.

Nevertheless, it's imperative to acknowledge the associated risks. Foremost among them is the exposure to radiation, which, albeit in substantial doses, can potentially jeopardize cellular integrity. The inherent resolution of X-ray imaging can sometimes prove insufficient for discerning subtle differences in soft tissues. Consequently, in specific clinical scenarios, alternative imaging methods might be necessitated for a more comprehensive diagnosis. X-rays offer an unparalleled view of dense structures like bones and tumors, facilitating the timely detection of fractures, select infections, and malignancies. Yet, despite its advantages, the ionizing radiation poses a heightened risk for certain populations, especially pediatric patients, emphasizing the need for judicious use. [32] [33]

The figure (4.1) below shows an example of an X-ray of an 80 year-old male with respiratory problems:

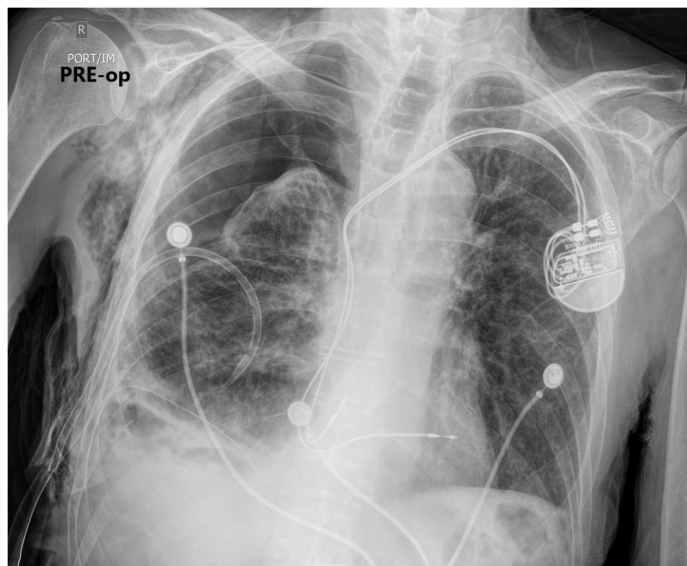


Figure 4.1: X-ray of a COPD case [3]

#### 4.1.2 Magnetic resonance imaging (MRI)

Over the course of its development, medical imaging has heralded a multitude of techniques, each tailored for specific therapeutic needs. While some modalities focus on detailed visualization of internal organs, others are more specialized, targeting areas like the brain or compromised bone tissues. Among these advancements, Magnetic Resonance Imaging (MRI) distinctly shines. MRI, a remarkable innovation in the medical imaging arena, utilizes magnetic fields to generate comprehensive images of the body's internal facets. Predominantly, it offers a deep view into soft tissues and has become a linchpin in diagnosing diverse conditions from cerebral anomalies to musculoskeletal disorders. Born in the latter part of the 20th century, MRI rapidly carved a niche for itself as a non-invasive alternative in medical diagnostics. Its operational principle revolves around the creation of a potent magnetic field that synchronizes the body's protons. Following this, radio frequency pulses disturb this alignment. As the protons revert, they release signals which are subsequently converted into detailed images. [34]

The unparalleled precision that MRI brings, especially in the realm of soft tissue imaging, makes it an irreplaceable tool in diagnostics. It stands out for its radiation-free methodology, accentuating patient safety. However, it's not devoid of challenges. Some individuals may find the MRI experience claustrophobic. Moreover, the existence of metallic implants has the potential to cause picture distortion, so compromising the sharpness of the image, and the procedure typically carries a higher cost compared to other imaging techniques. [35]

MRI uses a strong magnetic field and radio waves to produce details of internal structures of the body. The underlying mechanism relies on the interplay between magnetic fields and the protons present in the water molecules within the human body.

During an MRI exam, the patient is positioned inside a large, cylindrical magnet, and radio waves are directed towards the body. The alignment of protons inside the water molecules present in the human body occurs in response to the magnetic field, subsequently leading to their stimulation through the application of radio waves, producing a signal that is detected by a series of antennas. Subsequently, the acquired data is subjected to computational analysis in order to produce comprehensive visual representations of the underlying anatomical components.

The use of MRI is considered as a form of healthcare imaging that reveals particular proficiency in presenting the delicate tissues and organs within the human body, such as the brain, as an illustrative example. Additionally, it is employed for the purpose of identifying joint injuries, along with medical diseases such as neurological disorders. [36]

MRI was first developed in the 1970s, and it works by using strong magnetic fields and radio waves to generate and create accurate detailed images of the body's tissues. MRI produces very precise images that can show the structure and function of organs and tissues, including the brain and muscles. MRI is particularly useful for diagnosing neurological disorders, such as multiple sclerosis, as well as injuries to the musculoskeletal system. MRI images can be analyzed using techniques such as Fourier transform and wavelet transform to extract features and detect abnormalities.

One of the major benefits of MRI is its ability to produce clear images with excellent contrast between different types of soft tissues. Additionally, MRI does not use the harmful ionizing radiation, making it a safer option for certain patients, such as pregnant women or children. [37]

Furthermore, the utilisation of MRI often causes minimal discomfort to patients, while avoiding the exposure to radiation. MRI possesses the capability to aid in the identification and therapeutic guidance of various health conditions. Additionally, MRI can offer identical information to CT in some investigative scenarios. However, there are some downsides to using MRI imaging, such as its high cost and limited availability compared to other imaging modalities. Additionally, MRI exams can take longer to perform than other imaging modalities, which can be uncomfortable for some patients. Finally, some patients may not be able to undergo an MRI exam due to the presence of metallic implants, which can be affected by the strong magnetic field. [38] [30] [35]

The drawbacks of MRI might exhibit variability, with several factors contribut-

ing to these limitations. MRI is characterised by its protracted duration and the presence of substantial auditory disturbances, rendering even the most minor motion capable of compromising the resulting image. Retesting is necessary and may induce feelings of claustrophobia in certain individuals. Furthermore, the use of anaesthesia may be necessary for paediatric patients or individuals. Finally, the administration of injections, if deemed necessary, may potentially induce renal complications or elicit allergic responses in certain patients. Consequently, there are circumstances in which MRI cannot be conducted, such as the presence of a cardiac pacemaker. [37] [39] [30]

This figure(4.2) below shows example of what an MRI scan would appear like:

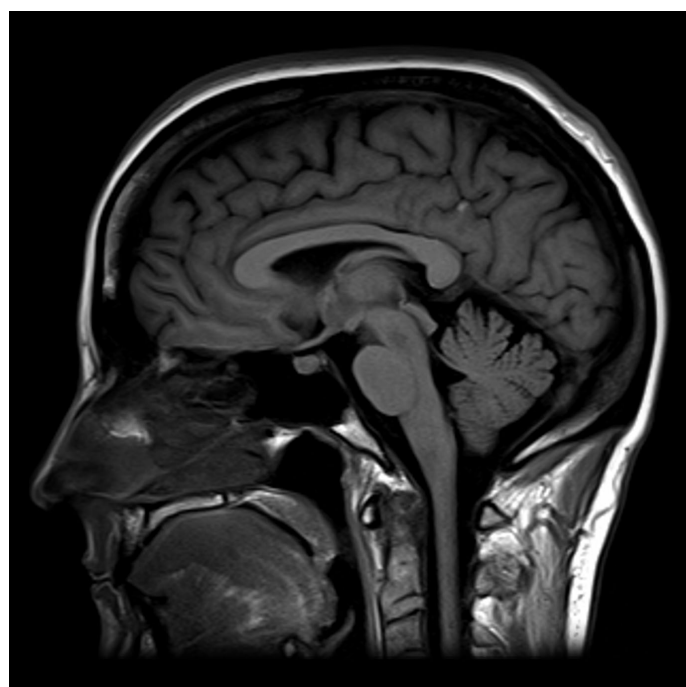


Figure 4.2: MRI of a normal brain [4]

### 4.1.3 Computed tomography (CT)

CT scanning is a medical imaging modality that utilises X-rays and computational algorithms to generate accurate visual representations of the internal anatomical structures of the human body. It is based on the principle of X-ray absorption by different tissues. During a CT scan, the patient lies on a table that moves through a circular opening in the CT machine. X-ray beams are directed towards the body from different angles, and detectors on the opposite side of the machine measure the quantity of X-rays that traverse

the human body. Subsequently, the acquired data from the detectors is subjected to computational analysis in order to produce a comprehensive three-dimensional representation of the interior components. [40]

CT scan stands as an innovative medical imaging procedure, harnessing the power of X-rays combined with advanced computing to yield intricate visuals of the body's inner architecture. It operates on the fundamental principle where varying tissues absorb X-rays differently. During CT, patients rest on a moving table that journeys through the CT apparatus's circular structure. X-ray emissions target the body from multifarious angles, while corresponding detectors gauge the X-ray quantities that traverse the body. The captured data undergoes sophisticated computational processing, culminating in a comprehensive 3D depiction of the internal organs.

Originating in the 1970s, CT scans diverge from conventional X-ray techniques. Rather than a singular 2D snapshot, CT produces a continuum of images, amalgamated to render a 3D representation. It can effectively diagnose cancers, injuries, and other issues. These images, under analytical lenses like the Radon transform, can further decode the original from its projections.

CT scans shine for their meticulous detailing, offering layers of cross-sectional visuals, capturing bones and tissues. This granularity extends its diagnostic purview far beyond traditional X-rays, serving as a diagnostic tool. Moreover, it acts as a sentinel, identifying potential resurgence of previously treated ailments. However, the CT modality doesn't come without reservations. Primarily, the risk of future oncological issues due to radiation exposure. Its radiation dosage surpasses that of standard X-rays, intensifying the associated risks. Moreover, certain protocols require the injection of a contrast medium, which, although pivotal, might instigate complications or allergic manifestations. Some procedures even need anesthesia, which can be daunting for patients. [41] [42]

This figure (4.3) below shows an example of CT scan images:

#### **4.1.4 Ultrasound images**

Ultrasound is known to be a non-invasive imaging modality for medical imaging that use high-frequency sound waves to provide visual representations of interior organs within the human body. It is based on the principle of sound wave propagation, reflection, and absorption. [30]

Ultrasound imaging entails the utilisation of a compact handheld apparatus known as a transducer, which releases sound waves of elevated frequency that enter the human organism and then reflect off the internal anatomical

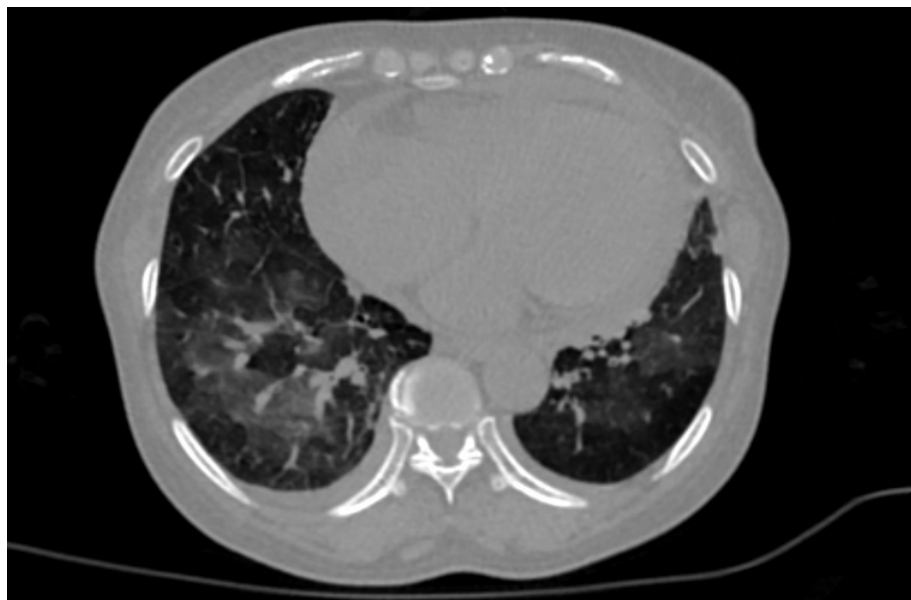


Figure 4.3: CT scan during Covid19 [5]

formations. These reflected sound waves are then detected by the transducer and converted into an image by a computer.

Ultrasound is widely used in medical imaging and is particularly specialized in obstetrics and gynecology, where it is used to monitor fetal growth and development, detect abnormalities in the uterus and ovaries, and diagnose conditions such as ectopic pregnancies and ovarian cysts. It is also used to image the heart and blood vessels, the liver, gallbladder, the kidneys and other organs and tissues.

The utilisation of ultrasound was initially implemented during the 1940s, employing high-frequency sound waves to generate visual representations of bodily tissues. The sound waves are emitted by a small probe that is placed on the skin, and the resulting image shows the relative density of the different tissues. Ultrasound is commonly used to monitor fetal development during pregnancy, as well as to diagnose conditions such as gallstones and kidney stones. Ultrasound images can be analyzed using signal processing techniques such as filtering and spectral analysis to extract information about tissue properties. [30]

One of the primary advantages of ultrasound imaging is in its non-invasive nature which makes it a safe imaging technique for pregnant women and paediatric populations. However, there are some downsides to using this technique, such as its limited ability to penetrate bone and air-filled organs, which can make it less effective in some cases. Additionally, ultrasound imaging is operator-dependent and can produce variable results depending on the skill and experience of the technician performing the exam. Finally, ultrasound

imaging is not suitable for all medical conditions, and other imaging modalities such as MRI and CT may be required in some cases. [6]

This figure (4.4) below shows an example of an ultrasound image of the liver:

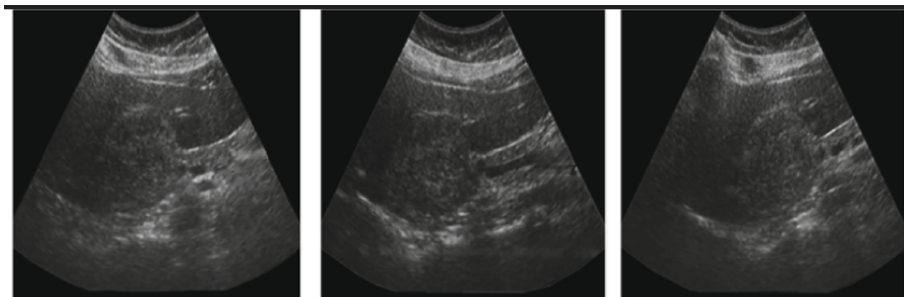


Figure 4.4: Ultrasound of the liver [6]

#### 4.1.5 Positron emission tomography (PET)

PET scanning is an imaging technique mostly employed in the field of cancer. Radiotracers are employed for the quantification of many metabolic processes within the human body. It has the capability to analyze a range of metabolic, and localised chemical alterations. Radioactive tracers can be administered via injection, ingestion, or inhalation, depending on the specific anatomical region under investigation. [43]

During a PET scan, the administration of the tracer can be achieved through intravenous, oral, or inhalation routes. Normally, the patient is injected with a small amount of a radioactive tracer, which emits positrons as it decays. When the positrons interact with the electrons located inside of the body, they produce gamma rays, which are captured by a gamma camera. Subsequently, the computer undertakes the processing of the data acquired from the gamma camera in order to build a three-dimensional representation of the specific organ or tissue that is being subjected to imaging. The PET machine features a centrally located aperture through which the patient is positioned. Typically, initial photographs serve as scout images to evaluate the accuracy of the location. Occasionally, there may be a necessity for the act of breath-holding. The duration of the scan typically ranges from half to one hour. [43]

PET is particularly specialized in oncology, neurology, and cardiology, where it is used to study the function and metabolism of the organs being imaged. It is also used to detect and stage cancers, monitor treatment response, and assess the risk of heart disease.

PET was initially developed during the 1970s, and it works by using a small amount of a radioactive tracer to detect metabolic activity in the body. The patient receives an intravenous injection of the tracer. Afterwards, a special camera detects the emissions of positrons from the tracer. The resulting image shows areas of increased metabolic activity, which can be used to diagnose cancer and other conditions. PET images can be analyzed using statistical methods to identify areas of increased metabolism.

PET entails the administration of a radioactive "tracer" through injection, inhalation, or ingestion [30]. Commonly utilised tracers encompass fluorine-18 (18F) fluoro-deoxyglucose (FDG), from which the term FDG-PET originates. This technique is employed for the purposes of diagnosing, staging, and monitoring several types of malignancies, with a special focus on Hodgkin's lymphoma. Moreover, it plays a significant role in identifying the presence of recurrent cervical cancer in both symptomatic and asymptomatic individuals. [43]

The scanner utilises gamma-rays generated by tracers to generate visual representations of bones and organs. This approach is advantageous due to its characteristic of being frequently devoid of discomfort, hence facilitating the diagnosis and prognostication of a diverse array of medical disorders. In contrast to several other imaging modalities, PET exhibits the capability to identify abnormalities at an earlier stage and provides insights into the functional dynamics of distinct anatomical regions. [30]

Finally, PET is involved with the assessment of cancer metastasis and the treatment efficacy which can be conducted to determine the extent of cancer progression and the effectiveness of therapeutic interventions [30]. Since the sensitivity of PET in detecting recurrent disease in asymptomatic women was found to be 80%, while the specificity was 100% which is crucial studying a tumor progression of a body tissue. [30]

One of the major benefits of PET imaging is its ability to provide functional and metabolic information about the organ or tissue being imaged, which cannot be obtained from other imaging techniques such as MRI or CT. Additionally, PET can detect changes in the organ or tissue's metabolism before structural changes are visible on other imaging modalities. [43]

Nevertheless, the utilisation of PET imaging is accompanied by certain drawbacks, including its substantial financial burden and the prerequisite for administering a radioactive tracer to the patient. Furthermore, it exhibits a very limited spatial resolution and is susceptible to motion and potentially compromising its precision. Ultimately, it should be noted that PET imaging may not be universally applicable to all medical disorders, and this might require the use of alternative imaging techniques in certain instances. Moreover, PET

scanners have been found to induce feelings of claustrophobia in certain individuals.

One final potential drawback of employing this technique is the inherent risk of radiation exposure, as the presence of radioactive material can potentially induce allergic or injection-site reactions in certain individuals. However, in general, the administration of radio-tracers is not associated with any notable adverse effects. [43]

This figure (4.5) below shows an example of an PET scan of head and neck cancer. The image located in the upper left quadrant depicts a distinct CT scan that showcases the anatomical structures. The scan located in the upper right quadrant displays PET-CT scans, wherein fake colour has been incorporated to facilitate the interpretation of the image. The initial FDG-PET imaging in the bottom left quadrant reveals the presence of tracer hot spots in the cervical area and a lymph node located in the right mandibular area, indicative of cancerous activity. The image seen in the lower right quadrant depicts a delayed enhancement scan, wherein the uptake of a tracer substance is observed over a period of time. This scan reveals the presence of typical areas of increased metabolic activity. [7]

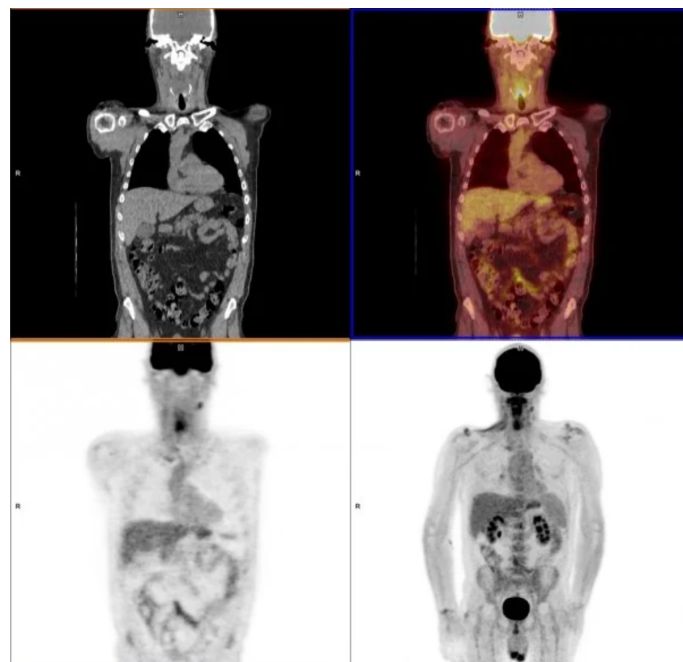


Figure 4.5: PET scans image example [7]

#### **4.1.6 Single-photon emission computed tomography (SPECT)**

Similarly to PET, SPECT is a medical imaging technology which utilises radioactive tracers and gamma rays for producing three-dimensional images of internal organs and tissues. It is based on the principle of photon emission and detection.

During a SPECT scan, a patient is administered a minimal dose of a radioactive tracer substance. This tracer substance undergoes radioactive decay, emitting gamma rays in the process. The gamma rays are detected using a gamma camera, which undergoes rotational movement around the patient, thereby acquiring images from various perspectives. Subsequently, the data acquired from the gamma camera is subjected to computational analysis in order to produce a three-dimensional representation of the specific organ or tissue under examination. [44]

The primary application of the SPECT scan is to assess individuals who are suspected of having dementia since it is primarily employed in the fields of neurology and psychiatry, wherein it is utilised for the examination of cerebral activity and the identification of ailments such as Alzheimer's and Parkinson's diseases. Moreover, it is applied in the investigation of brain perfusion patterns during surgical operations. Additionally, it is employed for cardiac imaging purposes, facilitating the identification of ailments like as coronary artery disease and myocardial infarction. [44]

One of the primary advantages associated with SPECT imaging is in its capacity to furnish functional data pertaining to the organ or tissue under examination, a capability that is not attainable through alternative imaging modalities such as MRI or CT. Furthermore, it should be noted that SPECT is also considered as a non-invasive imaging technique that carries a relatively low probability of radiation exposure. [44]

SPECT imaging is similar to PET imaging, but it uses a different type of radioactive tracer that emits gamma rays instead of positrons. The images obtained from this process have the potential to be utilised for the purpose of diagnosing medical disorders, including but not limited to heart disease and specific forms of cancer. SPECT images can be analyzed using similar methods to PET to identify areas of increased activity.

However, there are some downsides to using SPECT imaging, such as its limited spatial resolution and the need for the patient to be injected with a radioactive tracer. Additionally, SPECT imaging is characterised by an extended time frame and demands the patient's constant stillness which can be uncomfortable for some patients. Finally, SPECT imaging is not suitable for all medical conditions, and other imaging modalities may be required in some cases.

Each type of medical imaging has its own strengths and weaknesses. Doctors and radiologists may choose one technique over another depending on the specific condition being diagnosed or monitored. By combining multiple types of imaging, doctors can get a full overview and a comprehensive perspective of a patient's health and make more accurate diagnoses and treatment plans.

The illustration in (4.6) below is a 3D SPECT presentation of the liver:

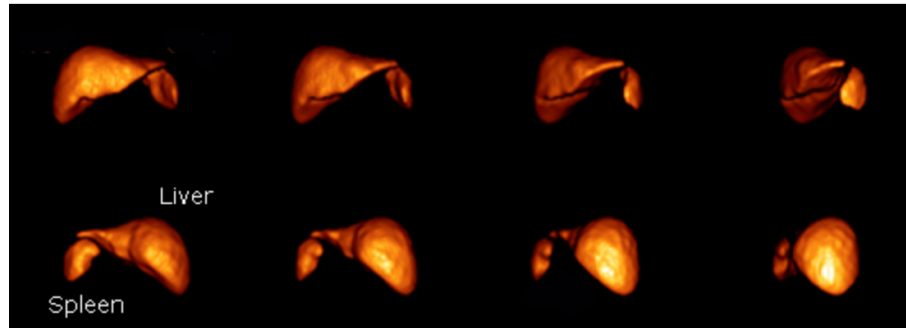


Figure 4.6: SPECT 3D for liver [8]

# 5

## Technical chapters

---

### 5.1 Reconstructing medical imaging using transforms

Reconstructing medical images plays a great role in modern medical medicine. Many studies have shown that reconstruction is implemented in one of four ways. The first method is using analytical methods like filtered back projection, inverse Radon transform and Fourier transform and other methods. The second method is using iterative reconstruction methods and sensor statistics, which improves quality of these images by reducing the noise. Third method is using modified data acquisition methods to make the process faster and the fourth type is using pre-created mathematical designed models with data-driven or adaptive models that implements machine learning models. This thesis focuses on the first method using the inverse Radon transform to reconstruct multiple medical imaging types. [33]

### 5.2 Methodology

Our methodology in this thesis is based basically on utilising the inverse Radon transform to reshape the medical images from a randomly selected datasets of different types of images (CT scan, MRI, and PET), where each data set contains 44 images of DICOM image extension and calculating the mean squared error (MSE) as the main measurement to compare the accuracy and study the effectiveness of using this transformation within medical imaging visualization. The datasets used are derived partially from the Cancer Imaging Archive mentioned here. DICOM (Digital Imaging in Medicine) serves as the cornerstone for storing and transferring medical image datasets. To handle DICOM datasets effectively, utilizing pydicom is recommended. Within pydicom, the primary function for reading and parsing DICOM files is dcmread().

While this function originates from the pydicom.filereader module, it is also available upon importing the main pydicom package. [45] [46] [47]

The process is mainly constructed using Python Programming language and the assigned libraries related to it such as DICOM library.

### 5.2.1 Used algorithm

This pseudocode below provides a high-level overview of the process.

*Reconstruction algorithm using Radon Transform and its inverse:*

*1. INPUT:*

- *OriginalImage: The medical image to be transformed.*
- *Theta: Range of angles for the Radon transform (usually 0 to 180 degrees).*

*2. PROCESS:*

*2.1. Perform Radon Transform on OriginalImage to get the Sinogram:*

*Sinogram = RadonTransform(OriginalImage, Theta)*

*2.2. Reconstruct the image from the Sinogram using Inverse Radon Transform:*

*ReconstructedImage = InverseRadonTransform(Sinogram, Theta)*

*2.3. Compare the OriginalImage and ReconstructedImage:*

*2.3.1. Calculate Mean Squared Error (MSE):*

*MSE = Sum for all pixels [(OriginalImage(pixel) – ReconstructedImage(pixel))<sup>2</sup>] / Total number of pixels*

*3. OUTPUT:*

- *Sinogram: The projection data from the Radon transform.*
- *ReconstructedImage: The image reconstructed from the sinogram.*
- *MSE: The mean squared error between the original and reconstructed images.*
- *PSNR and SSIM accuracy measurements calculated*

*End Algorithm*

## 5.2.2 Python implementation

In this section, we detail the methodology employed to process medical images stored in the DICOM format. The primary aim is to extract the sinogram using the Radon transform, reconstruct the medical image using the inverse Radon transform, and subsequently compute the mean squared error (MSE) between the original and reconstructed images for evaluation purposes at first. [48]

### 1. Library importation

The essential libraries for the image processing pipeline are imported:

- `numpy`: For numerical operations and matrix manipulations and other data structures efficiently.
- `pydicom`: To read and parse DICOM medical images. [48]
- `os`: To handle file and directory paths since Jupyter notebook was used to store, access and load images virtually.
- `skimage.transform`: Contains the Radon and inverse Radon transform functions.
- `skimage.metrics`: Provides the mean squared error function for image comparison and procures specific functions tailored for image quality assessments.
- `matplotlib.pyplot`: This library is used in rendering many of visual plots and charts, as the main tool for our data visualization needs.
- `pandas`: The main library for data handling and manipulation, it is chosen to tabulate and present the final computed metrics.

### 2. DICOM image loading

A function named `load_dicom_image` is defined, which accepts the path of a DICOM file as an argument. It reads the DICOM file, checks if it contains image data, and the process of normalizing the pixel values is performed so values can lie between 0 and 1. If the DICOM does not have image data or the image is entirely blank, it returns `None`. Within this function:

- The DICOM file is read using `pydicom.dcmread()`.
- The presence of pixel data is checked, ensuring that the file is indeed an image.

- The pixel data, representing the image, is normalized to the range [0,1] for further processing.

### 3. Processing the image set

The `process_image_set` function processes all DICOM images within a given directory. The workflow inside this function is as follows:

- For every file in the specified directory, the DICOM image is loaded.
- If the file does not represent an image (as identified by the aforementioned `load_dicom_image` function), it is skipped.
- The Radon transform is applied to the image, producing a sinogram.
- The inverse Radon transform is subsequently applied to the sinogram, reconstructing the image.
- The Mean Squared Error between the original and the reconstructed image is computed and stored in a list.
- Both the original and reconstructed images are displayed side by side for visualization after loading.

### 4. Dataset path specification

Directories containing DICOM images for different modalities, namely CT, MRI, and PET scans, are specified. This function is invoked for each directory (which represents each image modality used here).

### 5. Image processing execution

The previously defined `process_image_set` function is applied to each modality's directory. After processing all images in a directory, the function returns a list of MSE values for that modality.

### 6. Result display

Finally, the average MSE value for each modality is computed and displayed using the `numpy.mean` function. This aids in assessing the effectiveness of the Radon and inverse Radon transforms in reconstructing the images across different imaging modalities and provides a quick summary of the reconstruction quality across all images used.

The primary objective is to assess the quality of reconstructed images using three key metrics: structural similarity index (SSIM), mean squared error (MSE), and the peak signal-to-noise ratio (PSNR).

In order to assess the level of quality, the original and reconstructed images are juxtaposed and three metrics (MSE, PSNR, SSIM) are computed. The nuances of each metric serve to capture different aspects of image fidelity.

Each metric value is stored in dedicated lists for subsequent statistical analysis. Post traversal of all files, the function calculates and returns the average values of MSE, PSNR, and SSIM, providing an aggregate measure of the reconstruction efficacy for the entire image set.

The metrics from all modalities are collated into a single dataframe using the pandas library. This structured format not only augments readability but also prepares the data for potential subsequent analysis or visualization.

## 7. **Visualization of accuracy metrics across imaging modalities**

The quantitative metrics computed for evaluating the fidelity of image reconstructions are visualized, which facilitates a direct comparison between the three primary medical imaging modalities: CT, MRI, and PET. Below is a sum up of the visualization process of accuracy results using the mentioned metrics above (MSE, PSNR, SSIM).

- **Data initialization**

The values for MSE, PSNR, and SSIM that were previously computed for each modality are initialized as lists. These serve as the primary datasets to be visualized.

- **Visualization details**

A set of professional colors is chosen for the bars representing each metric to enhance clarity and visual appeal. Additionally, specifications like bar width and positions are determined to structure the visualization appropriately.

- **Plotting the comparative bar chart**

A bar chart is chosen for this visualization to allow an intuitive comparison of the three metrics across the modalities. Each metric is represented by a distinct colored bar. Specifically:

- MSE is visualized using a Navy blue color, denoting its foundational role in evaluating reconstructions.
- PSNR, with its emphasis on peak signal values, is represented in Dark cyan.
- SSIM, focusing on structural aspects, is showcased in Olive green.

The Y-axis is transformed to a logarithmic scale, to ensure that metrics with lower values remain clearly visible. This scale also subtly emphasizes the relative differences between metrics.

- **Finalization and presentation**

A legend is incorporated to enhance the readability of the chart and presenting a cohesive visual comparison.

This visualization shown below in Figure (5.1) aids in discerning the subtle nuances between the modalities and offers a holistic overview of the reconstruction quality. While quantitative metrics provide a mathematical assessment, this visualization caters to the intuitive understanding and interpretation of the results.

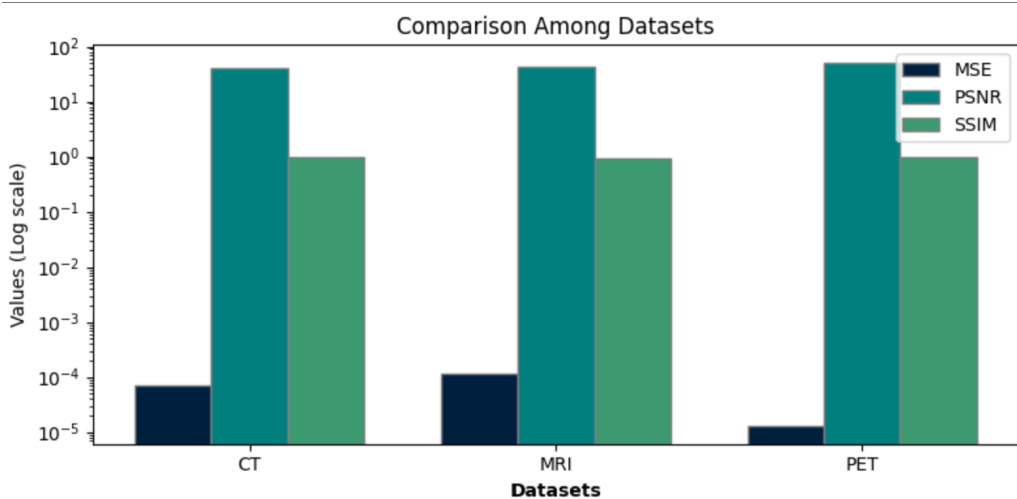


Figure 5.1: Accuracy metrics comparison.

# 6

## Results and discussions

---

### 6.1 Dataset used and description

In our thesis, we have used 3 datasets from the Cancer Imaging Archive website [10]

#### 6.1.1 CT dataset

First dataset used is CT pancreatic cancer. This dataset facilitates the evaluation of deformable registration between CT and cone-beam CT images, specifically for pancreatic cancer patients subjected to high-intensity radiation treatments. The aim is to enable the tracking of shifts in the location and form of organs at risk during therapeutic procedures. [49]

Data derives from 40 patients with "advanced pancreatic cancer treated at the Memorial Sloan Kettering Cancer Center" [49]. Each patient underwent ablative radiation therapy, with effective doses. [49]

#### 6.1.2 MRI breast cancer dataset

The dataset originates from the "American College of Radiology Imaging Network (ACRIN) trial 6698 (NCT01564368)" [46]. A multicenter endeavor evaluating the efficacy of "Diffusion Weighted Imaging (DWI) in gauging breast cancer response to neoadjuvant chemotherapy (NAC). This trial operated as a sub-study of the I-SPY 2 TRIAL" [46], a phase II trial targeting expedited identification of new agents for breast cancer therapy.

Between August 2012 and January 2015, "406 women with invasive breast cancer were enrolled at ten institutions" [46]. Out of these, "272 were randomized to I-SPY 2 experimental" [46] or control treatment groups.

Four MRI studies were executed over NAC treatment: pre-treatment, early-treatment, mid-treatment, and post-treatment. [46]

The dataset contains "all MRI studies sent to the UCSF image analysis lab, barring those with no analyzable captures". [46]

### 6.1.3 PET phantom dataset

This dataset encompasses "positron emission tomography (PET) phantom scans from the Quantitative Imaging Network's (QIN) PET Segmentation Challenge" [47]. The challenge aimed to gauge the variability in segmentations and the resultant quantitative analyses on phantom PET scans with established ground truth. Scans were conducted at "two QIN institutions (University of Iowa and University of Washington)" [47], utilizing diverse scanners. Adhering to a standardized protocol, each location generated four distinct image sets. [47]

## 6.2 Results

### 6.2.1 Interpretation of the mean squared error (MSE) results

The measure being referred to is a mathematical calculation that quantifies the average of the squared differences between the observed values and the projected values. Mainly used to determine the quality of the reconstruction by measuring how closely the reconstructed image is similar to the original image. A lower MSE value indicates that the reconstructed image is closer to the original image, and thus the reconstruction is of a higher quality.

Given the results:

1. **CT MSE average:**  $7.138675264229057 \times 10^{-5}$

The computed MSE for the CT images is relatively low, suggesting that the reconstructed images from the sinograms are very close to the original CT images. This implies that the Radon and inverse Radon transforms are effective for CT image reconstruction.

2. **MRI MSE average:**  $0.00011431090336860745$

The MSE for the MRI images is slightly higher than that of the CT images. Although still quite low, it suggests a slightly lesser fidelity in the reconstruction of MRI images compared to the CT images using the Radon and inverse Radon transforms. Nonetheless, the difference is minor, and the

reconstructions are likely still of high quality.

### 3. PET MSE average: $1.2699035391386853 \times 10^{-5}$

The PET images have the lowest MSE among the three modalities. This indicates that the reconstructed PET images from the sinograms are extremely close to the original PET images. The Radon and inverse Radon transforms seem to be highly effective in reconstructing PET images, even more so than CT and MRI.

**Overall**, the Radon and inverse Radon transforms have demonstrated efficacy in the reconstruction of medical images across the three modalities. The extremely low MSE values signify that the reconstructions are of high quality, with the PET reconstructions being particularly impressive. However, it's essential to consider the clinical relevance and acceptable error margins for each modality in a real-world setting, as even minor discrepancies might have significant implications in medical diagnosis and treatment planning.

#### 6.2.2 Interpretation of accuracy

1. **MSE (Mean Squared Error):** The metric calculates the mean squared deviation between the original and reconstructed pictures. Lower values indicate a closer match to the original image, implying better reconstruction accuracy. [50]
2. **PSNR (Peak Signal-to-Noise Ratio):** The ratio between the greatest achievable signal power and the power of the interfering noise is quantified. Higher values denote better image quality. [50]
3. **SSIM (Structural Similarity Index Measure):** Evaluates perceived changes in structural information, and texture between two images. A value of 1 indicates the two images being compared are identical, with values approaching 0 indicating vast discrepancies.

### 6.3 Results interpretation

#### 6.3.1 CT scan

MSE: 0.000071 (A very low value, indicating minimal error in reconstruction)

PSNR: 41.467276 (High quality reconstruction with low noise)

SSIM: 0.993951 (Close structural match with the original image)

### **6.3.2 MRI scan**

MSE: 0.000114 (Good reconstruction with slightly more error than CT)

PSNR: 43.487753 (Even better image quality than CT)

SSIM: 0.946154 (Some structural information might have been lost)

### **6.3.3 PET scan**

MSE: 0.000013 (Extremely accurate reconstruction)

PSNR: 49.970416 (Highest image quality with least noise among the three)

SSIM: 0.996293 (Excellent structural integrity)

## **6.4 Discussions**

As shown in the results above, the Radon and inverse Radon transform were most successful in reconstructing PET scans, with CT scans following closely, and MRI scans showing slightly more error and less structural similarity compared to the other two. However, all three modalities yielded good reconstruction results.

The used methodology in this thesis offers a structured approach to process and evaluate the quality of reconstructed medical images using the Radon transform and its inverse. It ensures efficient processing by skipping non-image DICOM files -if found- and normalizing image pixel values. This analysis is valuable for assessing the utility and accuracy of Radon transform-based reconstructions in medical imaging.

One of the things that needs to be taken into consideration while dealing with medical data is that datasets might not always behave the way expected and the results will always need improvements such as, being able to do the check-ups and upload the data and results in real time and have a unified dataset for each disease, because this type of solution will help analysts and scientists to provide more accuracy during the time of the study. Another suggestion is to keep in mind that medical datasets resources are not always available fully due to the privacy of patients and sensitivity of the data which might be an obstacle in the way of analyzing medical images using mathematical techniques.

# 7

## Conclusions & future work

---

### 7.1 Conclusions and results

In this thesis, the actual work was to identify and get to know the used mathematical transforms used in the medical imaging field. We got to know more regarding the Fourier transform, medical imaging modalities and how to use the inverse Radon transform to reconstruct medical images as a part of data visualization in the medical field and for our thesis we have used three modalities (MRI, CT scans and PET).

The evolving domain of medical imaging offers a myriad of challenges and opportunities. Among the advanced techniques available, the utilization of the Radon and inverse Radon transform to reconstruct medical images provides a promising pathway to enhance the clarity, accuracy, and efficacy of imaging modalities such as MRI, CT, and PET scans.

1. **Accuracy and image quality:** Our extensive comparative analysis across CT, MRI, and PET modalities showcased promising results. Specifically, the derived metrics such as MSE, PSNR, and SSIM provide quantitative evidence of the effectiveness of the Radon-based image reconstruction. PET scans, for instance, demonstrated remarkable fidelity in the reconstructed images, as indicated by its low MSE, high PSNR, and near-perfect SSIM.
2. **Versatility across modalities:** The adaptability of the Radon transform techniques across various imaging modalities reaffirms its versatile application potential. While each imaging technique (CT, MRI, and PET) has its own characteristics and challenges, the consistent performance of the Radon transforms underlines its broad-spectrum utility.
3. **Implications for clinical diagnostics:** Given the observed image fidelity, there is potential for these reconstruction methods to improve clinical

diagnostics. Clearer and more accurate images can lead to more definitive diagnoses, reduced ambiguities, and ultimately, better patient care.

4. **Visualization enhancements:** The use of advanced visualization techniques, as exhibited in the bar chart comparisons, not only facilitates better interpretation of results but also aids in presenting complex data in an easily digestible format. This is crucial for interdisciplinary collaborations where professionals from diverse backgrounds engage with the data.
5. **Future directions:** While the results are encouraging, further research can focus on optimizing the parameters involved in the Radon and inverse Radon transforms for each specific modality. Additionally, leveraging machine learning algorithms in tandem with these transforms could open new avenues for enhancing image quality further.

In summary, the Radon and inverse Radon transforms methods present a promising tool in the arsenal of medical imaging techniques. Their ability to significantly enhance the quality of reconstructed images from diverse modalities underscores their potential. As we continue to push the boundaries of medical imaging, such methodologies will undoubtedly play a pivotal role in shaping the future landscape of diagnostic medicine.

## 7.2 Challenges within this work

Throughout the progression of this study, several challenges emerged that warranted meticulous attention and iterative refinements in our methodology. Here's a comprehensive breakdown:

1. **Complexities with coloured images:** Initially, processing coloured images, particularly those employing the RGB system, posed substantial challenges. Such images inherently have a more intricate structure compared to the standard DICOM format typically used in medical imaging. DICOM images, rendered primarily in shades of black and white, are simpler to interpret and read, especially when applying mathematical transforms. Notably, the inverse Radon transform's application on coloured images was particularly intricate due to these complexities.
2. **Ineffective reconstruction approaches:** Our early attempts at image reconstruction incorporated multiple methodologies that proved sub-optimal. One such approach, which involved extracting density values from medical image histograms, yielded inconsistent results. The reconstructed images often exhibited high levels of noise. Moreover, the utilization of the *flatten()* function often led to the generation of images with indistinct edges, diminishing the clarity of reconstructed subjects.

3. **Disparities in reconstructed images:** While the application of the inverse Radon transform for reconstructing medical images is feasible, it doesn't guarantee an exact replication of the original images. This discrepancy became evident when assessing the fidelity of a reconstructed CT scan image against its original counterpart using the mean squared error (MSE) metric.
4. **Challenges with pixel extraction:** Our approach of extracting pixel values, storing them externally, and then applying the inverse Radon transform yielded results that often diverged from our anticipated outputs. Consequently, we pivoted towards leveraging the native functionalities provided by Python's radon and iradon libraries for a more consistent and reliable reconstruction process.
5. **Challenges in grasping advanced mathematical concepts in medical imaging:** Navigating the intricacies of certain mathematical principles reveals the profound depth required to understand the application of transforms in medical imaging. It's evident that this field, marked by its rapid advancements and continual innovations, demands an extended and dedicated study period. To genuinely contribute and influence this domain, a deep mastery and comprehensive understanding of the underlying mathematical frameworks are indispensable.

# Bibliography

---

- [1] S. Iqbal, A. N. Qureshi, J. Li, and T. Mahmood, "On the Analyses of Medical Images Using Traditional Machine Learning Techniques and Convolutional Neural Networks," *Archives of Computational Methods in Engineering*, vol. 30, no. 5, pp. 3173–3233, apr 4 2023.
- [2] Y. Zhang and Z. Dong, "Medical Imaging and Image Processing," *Technologies*, vol. 11, no. 2, p. 54, apr 5 2023.
- [3] L. Silverstone and D. Cummins, "Hydropneumothorax," *Radiopaedia.org*, aug 24 2023.
- [4] B. Di Muzio and F. Gaillard, "Normal midline brain (MRI)," *Radiopaedia.org*, may 21 2008.
- [5] "Ct Images in COVID-19 - The Cancer Imaging Archive (TCIA) Public Access - Cancer Imaging Archive Wiki," <https://doi.org/10.7937/TCIA.2020.GQRY-NC81>.
- [6] P. Singh, R. Mukundan, and R. De Ryke, "Texture Based Quality Analysis of Simulated Synthetic Ultrasound Images Using Local Binary Patterns," *Journal of Imaging*, vol. 4, no. 1, p. 3, dec 21 2017.
- [7] "Pet Scans Imaging 101," <http://www.itnonline.com/article/pet-scans-imaging-101>, jun 3 2016.
- [8] M. Lyra, "Single photon emission tomography (spect) and 3d images evaluation in nuclear medicine," in *Image Processing*, Y.-S. Chen, Ed. Rijeka: IntechOpen, 2009, ch. 15.
- [9] W. D. Bidgood, S. C. Horii, F. W. Prior, and D. E. Van Syckle, "Understanding and Using DICOM, the Data Interchange Standard for Biomedical Imaging," *Journal of the American Medical Informatics Association*, vol. 4, no. 3, pp. 199–212, may 1 1997.
- [10] "Tcia Collections - The Cancer Imaging Archive (TCIA)," <https://www.cancerimagingarchive.net/collections/>.
- [11] X. W. Gao, Y. Qian, and R. Hui, "The State of the Art of Medical Imaging Technology: from Creation to Archive and Back," *The Open Medical Informatics Journal*, vol. 5, no. 1, pp. 73–85, jul 27 2011.
- [12] H. Liao, S. K. Zhou, and J. Luo, *Deep Network Design for Medical Image Computing: Principles and Applications*, ser. The\MICCAI Society Book Ser. Academic Press, aug 24 2022.

- [13] M. Yaqub, F. Jinchao, K. Arshid, S. Ahmed, W. Zhang, M. Z. Nawaz, and T. Mahmood, "Deep Learning-Based Image Reconstruction for Different Medical Imaging Modalities," *Computational and Mathematical Methods in Medicine*, vol. 2022, pp. 1–18, jun 16 2022.
- [14] P. Rattey and A. Lindgren, "Sampling the 2-D Radon transform," *IEEE Transactions on Acoustics, Speech, and Signal Processing*, vol. 29, no. 5, pp. 994–1002, 10 1981.
- [15] H. H. Barrett, "lii the radon transform and its applications," ser. Progress in Optics, E. Wolf, Ed. Elsevier, 1984, vol. 21, pp. 217–286.
- [16] "Radon transform - Alchetron, The Free Social Encyclopedia," <https://alchetron.com/Radon-transform>, aug 18 2017.
- [17] K. Fang, "The Radon Transformation and Its Application in Tomography," *Journal of Physics: Conference Series*, vol. 1903, no. 1, p. 012066, apr 1 2021.
- [18] S. R. Deans, *The Radon Transform and Some of Its Applications*. Wiley-Interscience, jan 1 1982.
- [19] M. M. Ter-Pogossian, "Image Reconstruction from Projections, The Fundamentals of Computerized Tomography by G. T. Herman," *Medical Physics*, vol. 11, no. 1, pp. 90–90, 1 1984.
- [20] A. C. Kak, M. Slaney, and G. Wang, "Principles of Computerized Tomographic Imaging," *Medical Physics*, vol. 29, no. 1, pp. 107–107, 1 2002.
- [21] M. Barth, J. R. Reichenbach, R. Venkatesan, E. Moser, and E. Haacke, "High-resolution, multiple gradient-echo functional MRI at 1.5 T," *Magnetic Resonance Imaging*, vol. 17, no. 3, pp. 321–329, 4 1999.
- [22] M. Iorga, N. Schneider, J. Cho, M. C. Tate, and T. B. Parrish, "A novel intraoperative mapping device detects the thermodynamic response function," *Brain Sciences*, vol. 13, no. 7, 2023.
- [23] I. T. Jolliffe, *Principal component analysis for special types of data*. Springer, 2002.
- [24] W. J. Morgan and H.-Y. Chu, "An unsupervised vibration noise reduction approach and its application in lubrication condition monitoring," *Lubricants*, vol. 11, no. 2, 2023.
- [25] E. Uzeirbegovic, J. E. Geach, and S. Kaviraj, "Eigengalaxies: describing galaxy morphology using principal components in image space," *Monthly Notices of the Royal Astronomical Society*, vol. 498, no. 3, pp. 4021–4032, 09 2020.

- [26] P. C. Hansen, "Analysis of Discrete Ill-Posed Problems by Means of the L-Curve," *SIAM Review*, vol. 34, no. 4, pp. 561–580, 12 1992.
- [27] G. H. Golub and C. Reinsch, "Singular value decomposition and least squares solutions," *Numerische Mathematik*, vol. 14, no. 5, pp. 403–420, 4 1970.
- [28] C. F. Van Loan and G. Golub, "Matrix computations (johns hopkins studies in mathematical sciences)," *Matrix Computations*, vol. 5, 1996.
- [29] "Improving principal component analysis (PCA) in automotive body assembly using artificial neural networks," *Journal of Manufacturing Systems*, vol. 21, no. 6, p. 478, 1 2002.
- [30] "Imaging explained," <https://www.nps.org.au/consumers/imaging-explained>, dec 22 2016.
- [31] A. B. Wolbarst and W. R. Hendee, "The National Institute of Biomedical Imaging and Bioengineering and NIH Grant Process: An Overview," *Radiology*, vol. 242, no. 1, pp. 32–55, 1 2007.
- [32] V. Parot, C. Sing-Long, C. Lizama, C. Tejos, S. Uribe, and P. Irarrazaval, "Application of the fractional Fourier transform to image reconstruction in MRI," *Magnetic Resonance in Medicine*, vol. 68, no. 1, pp. 17–29, oct 17 2011.
- [33] S. Ravishankar, J. C. Ye, and J. A. Fessler, "Image Reconstruction: From Sparsity to Data-Adaptive Methods and Machine Learning," *Proceedings of the IEEE*, vol. 108, no. 1, pp. 86–109, 1 2020.
- [34] L. Warner, M. Kotys-Traughber, and U. Blume, "Su-E-I-136: Mr Imaging Techniques with Reduced Metal Artifact for Improved Brachytherapy Device Visualization," *Medical Physics*, vol. 38, no. 6Part6, pp. 3427–3427, 6 2011.
- [35] "nonrigid registration algorithm: Topics by Science.gov," <https://www.science.gov/topicpages/n/nonrigid+registration+algorithm>.
- [36] M. N. Farinha, C. S. Semedo, A. M. Diniz, and V. Herédia, "Individual and contextual variables as predictors of mri-related perceived anxiety," *Behavioral Sciences*, vol. 13, no. 6, 2023.
- [37] A. M. Owen and M. R. Coleman, "Functional MRI in disorders of consciousness: advantages and limitations," *Current Opinion in Neurology*, vol. 20, no. 6, pp. 632–637, 12 2007.
- [38] M. A. Foster, "Nuclear magnetic resonance spectroscopy," *Magnetic Resonance Imaging*, vol. 2, no. 3, pp. 254–255, 1 1984.

- [39] R. Zivadinov and T. P. Leist, "Clinical-Magnetic Resonance Imaging Correlations in Multiple Sclerosis," *Journal of Neuroimaging*, vol. 15, pp. 10S-21S, 10 2005.
- [40] G. W. Friedland and B. D. Thurber, "The birth of CT." *American Journal of Roentgenology*, vol. 167, no. 6, pp. 1365–1370, 12 1996.
- [41] S. Tan and P. Poole, "Allan MacLeod Cormack (1924–1998): Discoverer of computerised axial tomography," *Singapore Medical Journal*, vol. 61, no. 1, pp. 4–5, 1 2020.
- [42] M. Donya, M. Radford, A. ElGuindy, D. Firmin, and M. H. Yacoub, "Radiation in medicine: Origins, risks and aspirations," *Global Cardiology Science and Practice*, vol. 2014, no. 4, p. 57, 12 2014.
- [43] M. Kapoor and A. Kasi, "Pet Scanning - StatPearls - NCBI Bookshelf," <https://www.ncbi.nlm.nih.gov/books/NBK559089/>, oct 3 2022.
- [44] S. Yandrapalli and Y. Puckett, "Spect Imaging - StatPearls - NCBI Bookshelf," <https://www.ncbi.nlm.nih.gov/books/NBK564426/>, oct 3 2022.
- [45] J. Hong, M. Reyngold, C. Crane, J. Cuaron, C. Hajj, J. Mann, M. Zinovoy, E. Yorke, E. LoCastro, A. P. Apte, and G. Mageras, "Ct and cone-beam CT of ablative radiation therapy for pancreatic cancer with expert organ-at-risk contours," *Scientific Data*, vol. 9, no. 1, oct 21 2022.
- [46] D. C. Newitt, Z. Zhang, J. E. Gibbs, S. C. Partridge, T. L. Chenevert, M. A. Rosen, P. J. Bolan, H. S. Marques, S. Aliu, W. Li, L. Cimino, B. N. Joe, H. Umphrey, H. OjedaFournier, B. Dogan, K. Oh, H. Abe, J. Druktteinis, L. J. Esserman, and N. M. Hylton, "Test-retest repeatability and reproducibility of ADC measures by breast DWI: Results from the ACRIN 6698 trial," *Journal of Magnetic Resonance Imaging*, vol. 49, no. 6, pp. 1617–1628, oct 22 2018.
- [47] "Qin PET Phantom - The Cancer Imaging Archive (TCIA) Public Access - Cancer Imaging Archive Wiki," <https://wiki.cancerimagingarchive.net/display/Public/QIN+PET+Phantom>.
- [48] "pydicom documentation — pydicom 2.4.2 documentation," <https://pydicom.github.io/pydicom/stable/>.
- [49] "Breath-hold CT and cone-beam CT images with expert manual organ-at-risk segmentations from radiation treatments of locally advanced pancreatic cancer (Pancreatic-CT-CBCT-SEG) - The Cancer Imaging Archive (TCIA) Public Access - Cancer Imaging Archive Wiki," <https://wiki.cancerimagingarchive.net/pages/viewpage.action?pageId=93258557>.
- [50] N. Abbas and M. Abdulmunim, "mrna approach image encryption using luc algorithm," *Iraqi Journal of Science*, vol. 64, pp. 2545–2560, 05 2023.

# Appendix 1 - Implementation code

```
1 pip install matplotlib numpy scikit-image pydicom
2 import numpy as np
3 import pydicom # used library for the DICOM images
4 import os
5 from skimage.transform import radon, iradon # used library to
6     implement Radon and inverse Radon transform
7 from skimage.metrics import mean_squared_error # importing
8     mean squared error for calculating accuracy
9 #For graph and data visualization of the results
10 import matplotlib.pyplot as plt
11
12 def load_dicom_image(file_path):
13     ds = pydicom.dcmread(file_path)
14     if 'PixelData' not in ds:
15         return None
16
17     # extracting Pixel by pixel values of the image
18     image = ds.pixel_array
19     if np.max(image) == 0:
20         return None
21
22     image = image.astype(np.float) / np.max(image)
23     return image
24
25 # Extracting MSE values for each image
26 def process_image_set(folder_path):
27     mse_values = []
28
29     for file_name in os.listdir(folder_path):
30         file_path = os.path.join(folder_path, file_name)
31
32         #Loading DICOM images
33         image = load_dicom_image(file_path)
34
35         if image is None: # Skip non-image DICOM files
36             continue
37
38         # Radon and Inverse Radon Transform implementation
39         theta = np.linspace(0., 180., max(image.shape),
40             endpoint=False)
41         sinogram = radon(image, theta=theta)
42         reconstructed = iradon(sinogram, theta=theta)
```

```

40     # Computing MSE between original and reconstructed
41     # images
42     mse = mean_squared_error(image, reconstructed)
43     mse_values.append(mse)
44
45
46 # importing directories for CT, MRI, and PET scans from the
47 # drive
47 ct_folder = '/content/drive/MyDrive/Thesis/Dataset/CT'
48 mri_folder = '/content/drive/MyDrive/Thesis/Dataset/MRI'
49 pet_folder = '/content/drive/MyDrive/Thesis/Dataset/PET'
50
51 ct_mse = process_image_set(ct_folder)
52 mri_mse = process_image_set(mri_folder)
53 pet_mse = process_image_set(pet_folder)
54
55 print(f"CT MSE Average: {np.mean(ct_mse)}")
56 print(f"MRI MSE Average: {np.mean(mri_mse)}")
57 print(f"PET MSE Average: {np.mean(pet_mse)}")

```

**This code will perform the Radon transform to extract the sinogram from the original image, after that it will use the inverse Radon Transform to reconstruct the original image. Furthermore, it will print out the MSE, PSNR, and SSIM metrics for all used datasets in general, which can be used to gauge the quality of the reconstruction and similarity to the original image as shown in the firgure below:**

```

CT MSE Average: 7.138675264229057e-05
MRI MSE Average: 0.00011431090336860745
PET MSE Average: 1.2699035391386853e-05

```

Figure 7.1: MSE average for each dataset

# Appendix 2 - Plotting results with MSE

```
1 def load_dicom_image(file_path):
2     ds = pydicom.dcmread(file_path)
3
4     if 'PixelData' not in ds:
5         return None
6
7     image = ds.pixel_array
8     if np.max(image) == 0:
9         return None
10    image = image.astype(np.float64) / np.max(image)
11    return image
12
13
14 def process_image_set(folder_path):
15     mse_values = []
16
17     for file_name in os.listdir(folder_path):
18         file_path = os.path.join(folder_path, file_name)
19
20
21         image = load_dicom_image(file_path)
22
23         if image is None:
24             continue
25
26         # Radon and Inverse Radon Transform implementation
27
28         theta = np.linspace(0., 180., max(image.shape),
29                             endpoint=False)
29         sinogram = radon(image, theta=theta)
30         reconstructed = iradon(sinogram, theta=theta)
31
32         # Computing MSE between original and reconstructed
33         # images for each modality
34         mse = mean_squared_error(image, reconstructed)
35         mse_values.append(mse)
36
37         # Displaying the original and reconstructed images
38         # next to each other to figure our the differences
39         # and resemblance
40         plt.figure(figsize=(10, 5))
41         plt.subplot(1, 2, 1)
```

```

39     plt.imshow(image, cmap='gray')
40     plt.title('Original Image')
41     plt.axis('off')
42
43     plt.subplot(1, 2, 2)
44     plt.imshow(reconstructed, cmap='gray')
45     plt.title('Reconstructed Image')
46     plt.axis('off')
47
48     plt.suptitle(f"File: {file_name} | MSE: {mse:.4f}")
49     plt.tight_layout()
50     plt.show()
51
52     return mse_values
53
54 ct_folder = '/content/drive/MyDrive/Thesis/Dataset/CT'
55 mri_folder = '/content/drive/MyDrive/Thesis/Dataset/MRI'
56 pet_folder = '/content/drive/MyDrive/Thesis/Dataset/PET'
57
58 ct_mse = process_image_set(ct_folder)
59 mri_mse = process_image_set(mri_folder)
60 pet_mse = process_image_set(pet_folder)
61
62 print(f"CT MSE Average: {np.mean(ct_mse)}")
63 print(f"MRI MSE Average: {np.mean(mri_mse)}")
64 print(f"PET MSE Average: {np.mean(pet_mse)}")

```

***In this code, it processes each medical image, along with the reconstructed medical image and the MSE accuracy rate above them.***

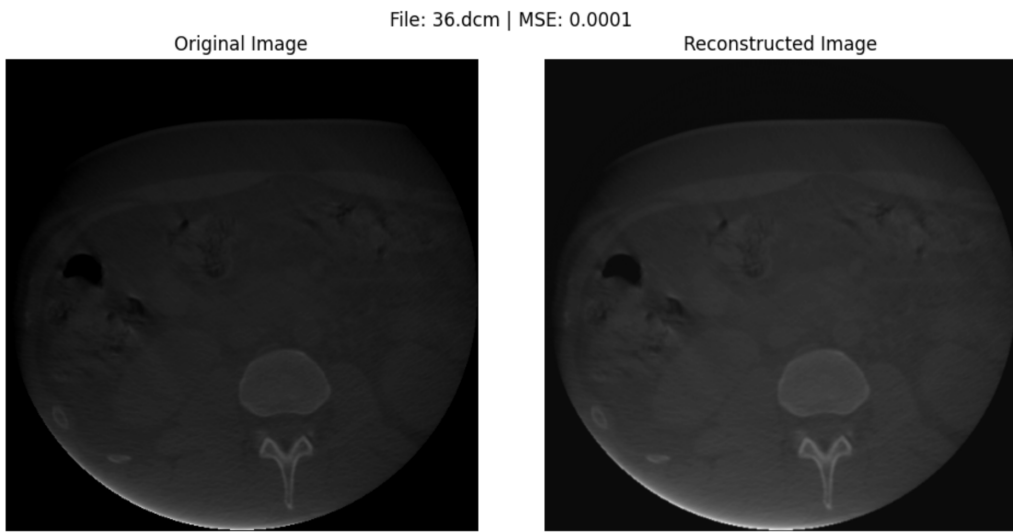


Figure 7.2: Original and reconstructed images results for CT

**Reconstructed CT scan image is lighter in contrast and there is some ambiguity in tissues presence but in general**

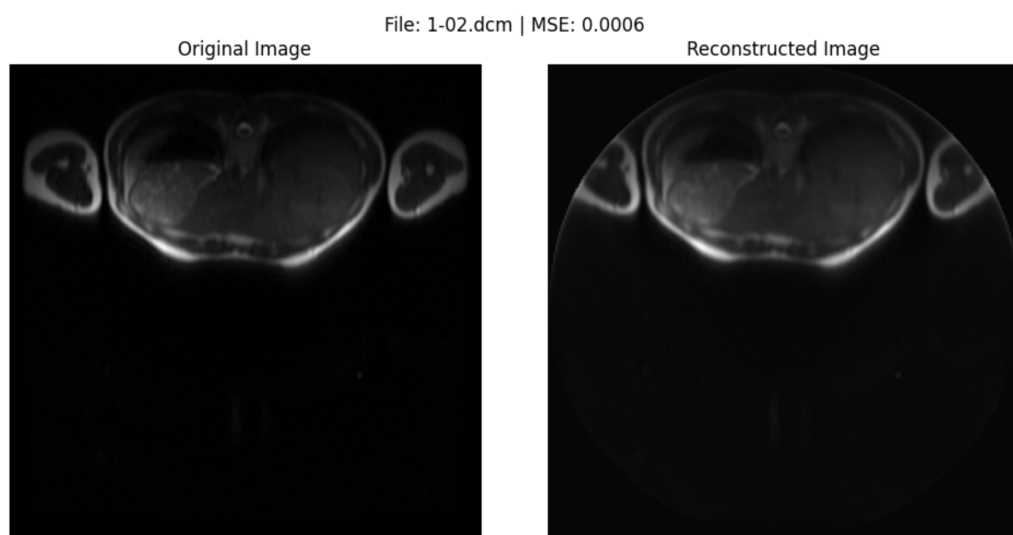


Figure 7.3: Original and reconstructed images results for MRI - example 1

**Reconstructed MRI image is less in volume from the edges**

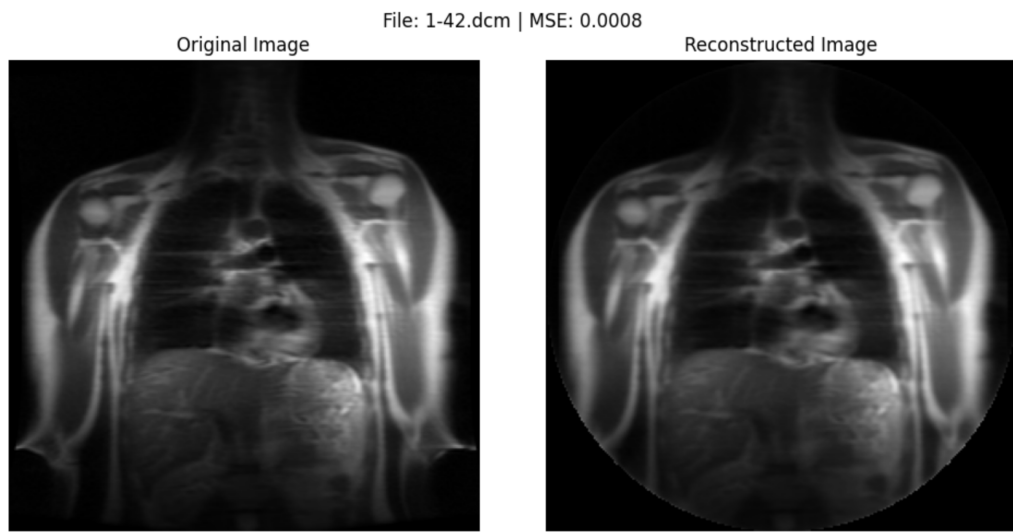


Figure 7.4: Original and reconstructed images results for MRI - example 2

**Reconstructed MRI image is not showing the entire edges with a higher MSE rate**

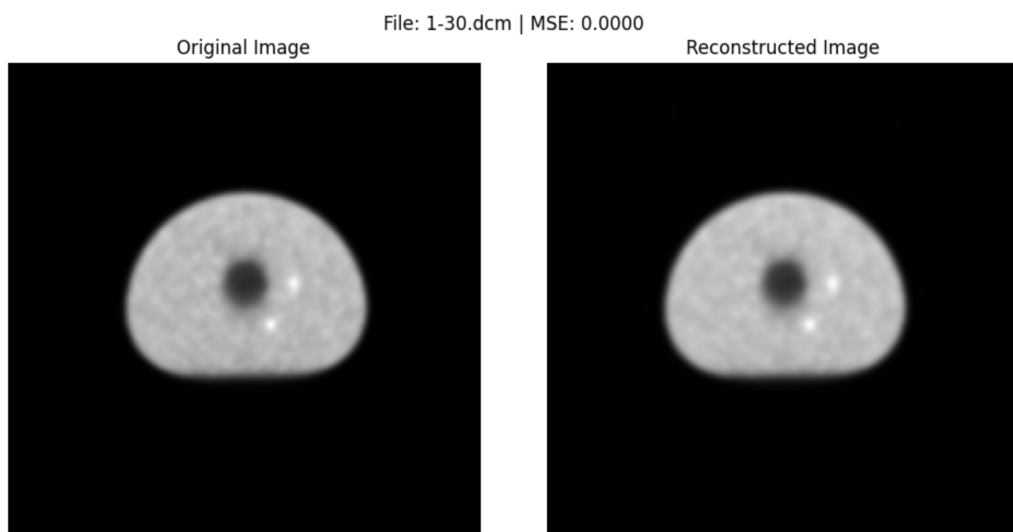


Figure 7.5: Original and reconstructed images results for phantom PET scan

**Reconstructed PET scan image is identical to the original image showing no noise or missing tissues**

# Appendix 3 - Statistical accuracy metrics used

```
1 #importing the needed libraries for accuracy metrics
2 #                           calculation
3 from skimage.metrics import mean_squared_error,
4     peak_signal_noise_ratio, structural_similarity
5 import pandas as pd
6
7 def load_dicom_image(file_path):
8     ds = pydicom.dcmread(file_path)
9
10    if 'PixelData' not in ds:
11        return None
12
13    image = ds.pixel_array
14    if np.max(image) == 0:
15        return None
16    image = image.astype(np.float64) / np.max(image)
17    return image
18
19 def process_image_set(folder_path):
20     mse_values, psnr_values, ssim_values = [], [], []
21
22     for file_name in os.listdir(folder_path):
23         file_path = os.path.join(folder_path, file_name)
24
25         image = load_dicom_image(file_path)
26
27         if image is None: files
28             continue
29
30         # Radon and Inverse Radon Transform
31         theta = np.linspace(0., 180., max(image.shape),
32                             endpoint=False)
33         sinogram = radon(image, theta=theta)
34         reconstructed = iradon(sinogram, theta=theta)
35
36         # Compute metrics
37         mse = mean_squared_error(image, reconstructed)
38         psnr = peak_signal_noise_ratio(image, reconstructed,
39                                         data_range=image.max() - image.min())
40         ssim = structural_similarity(image, reconstructed,
41                                     data_range=image.max() - image.min())
```

```

38     mse_values.append(mse)
39     psnr_values.append(psnr)
40     ssim_values.append(ssim)
41
42     return np.mean(mse_values), np.mean(psnr_values), np.mean
43         (ssim_values)
44
45 ct_folder = '/content/drive/MyDrive/Thesis/Dataset/CT'
46 mri_folder = '/content/drive/MyDrive/Thesis/Dataset/MRI'
47 pet_folder = '/content/drive/MyDrive/Thesis/Dataset/PET'
48
49 ct_metrics = process_image_set(ct_folder)
50 mri_metrics = process_image_set(mri_folder)
51 pet_metrics = process_image_set(pet_folder)
52
53 # Creating a table using pandas to present each metric value
54 # for each modality
55 df = pd.DataFrame({
56     'Modality': ['CT', 'MRI', 'PET'],
57     'MSE': [ct_metrics[0], mri_metrics[0], pet_metrics[0]],
58     'PSNR': [ct_metrics[1], mri_metrics[1], pet_metrics[1]],
59     'SSIM': [ct_metrics[2], mri_metrics[2], pet_metrics[2]]})
60
61 print(df)

```

**This part is to calculate the MSE, PSNR and SSIM for each used dataset type and present them in a table format as showed in this figure below:**

	Modality	MSE	PSNR	SSIM
0	CT	0.000071	41.467276	0.993951
1	MRI	0.000114	43.487753	0.946154
2	PET	0.000013	49.970416	0.996293

Figure 7.6: MSE, PSNR and SSIM accuracy

# Appendix 4 - Plotting accuracy results

```
1 import matplotlib.pyplot as plt
2 import numpy as np
3
4 datasets = ["CT", "MRI", "PET"]
5 mse_values = [0.000071, 0.000114, 0.000013]
6 psnr_values = [41.467276, 43.487753, 49.970416]
7 ssim_values = [0.993951, 0.946154, 0.996293]
8
9 # we will use the professional colors of Navy blue, Dark Cyan
10 # , and Olive green for display
11 colors = ["#001F3F", "#007F7F", "#3D9970"]
12
13 # Bar chart positioning
14 barWidth = 0.25
15 r1 = np.arange(len(mse_values))
16 r2 = [x + barWidth for x in r1]
17 r3 = [x + barWidth for x in r2]
18
19 plt.figure(figsize=(8, 4))
20
21 # Creating bars for each metric
22 plt.bar(r1, mse_values, color=colors[0], width=barWidth,
23         edgecolor='grey', label='MSE')
24 plt.bar(r2, psnr_values, color=colors[1], width=barWidth,
25         edgecolor='grey', label='PSNR')
26 plt.bar(r3, ssim_values, color=colors[2], width=barWidth,
27         edgecolor='grey', label='SSIM')
28
29
30 plt.title('Comparison Among Datasets')
31 plt.xlabel('Datasets', fontweight='bold')
32 plt.xticks([r + barWidth for r in range(len(mse_values))], [
33     'CT', 'MRI', 'PET'])
34
35 # Using a logarithmic scale for better visibility of all
36 # measurements
37 plt.yscale('log')
38 plt.ylabel('Values (Log scale)')
39
40 plt.legend()
41 plt.tight_layout()
42 plt.show()
```

**This part is to calculate the MSE, PSNR and SSIM among all data sets and present them in a plot format as showed in this figure below:**

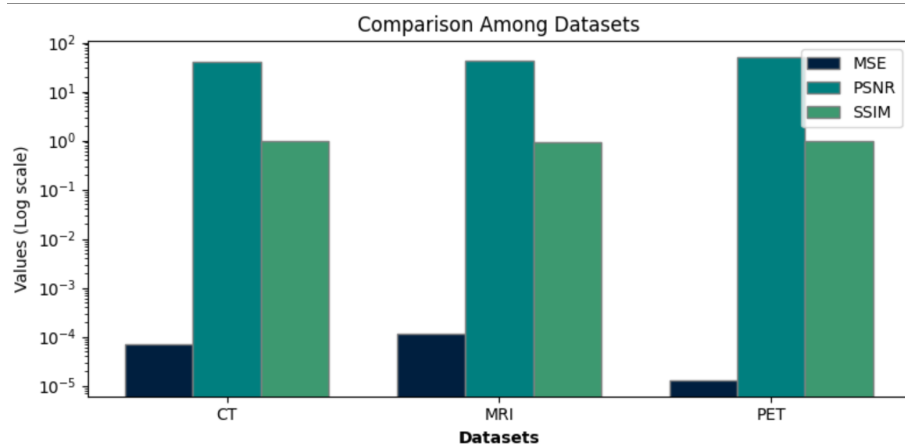


Figure 7.7: Accuracy measurement among datasets